

Topology Geometrics for the Generation of the Roccustyrnatm Molecule, A Ligand Targeted Covid-19-D614g Sites

Grigoriadis Ioannis

Biogenea Pharmaceuticals Ltd, Pharmaceutical Biotechnology Company, Thessaloniki, Greece

Abstract

SARS coronavirus 2 (SARS-CoV-2) encoding a D614G mutation in the viral spike (S) protein predominate over time in locales where it is found, implying that this change enhances viral transmission. It has also been observed that retroviruses pseudotyped with SG614 infected ACE2-expressing cells markedly more efficiently than those with SD614. The availability of newer modeling techniques, powerful computational resources, and good-quality data have made it possible to generate reliable predictions for new chemical entities, impurities, chemicals, natural products, and a lot of other substances fuelling further development and growth of the field to balance the trade-off between the molecular complexity and the quality of such predictions that cannot be obtained by any other method. In this article, we effectively use a decision tree to obtain an optimum number of small chemical active chemical features from a collection of thousands of them utilizing a shallow neural network and jointly free energy cumulative feature ranking method with decision tree taking both network parameters and input toxicity benchmark features into account. In this paper, we strongly combine the toxic models and ADMET methods that are simple in machine learning characteristics, efficient in computing resource usage, and powerful to achieve very high accuracy levels for the in-silico generation of the Roccustyrna™ small molecule, a less toxic nano-ligand targeted the COVID-19-D614G mutation using Topology Euclidean Geometric and Artificial Intelligence-Driven Predictive Neural Networks. To demonstrate this, we also develop a Gravitational Topological (UFs) based Quantum-Parallel Particle Swarm Inspired framework using only 2D chemical features that are less compute-intensive.

Keywords: COVID19 •D614G •Gravitational •Topological •AI-Quantum computing •Entanglement complexity computability •Quantum-inspired evolutionary algorithm predictive toxicology •QSAR •Artificial intelligence •Data mining •Machine learning •Data driven •Learning •Cheminformatics

Introduction

The COVID-19 disease was declared on March 2020 a pandemic by the World Health Organization (WHO) and is accountable for a large number of fatal cases. [1-4] On January 2020, WHO emergency committee declared a global health emergency [3,4-6] based on the rate of increasing spread of the infection [4-7] with a reproductive number (RN) in the range 2.0-6.5, 4 higher than SARS and MERS, [8] with more than 85,000 casualties and fatality rate of about 4%. [1-4] Collaborative efforts for Genomic characterization, [5-9] Molecular epidemiology, evolution, phylogeny of SARS coronavirus and epidemiology from scientists worldwide are underway to understand the rapid spread of the novel coronavirus (CoVs), and to develop effective interventions for control and prevention of the disease. [1-10] Coronaviruses are positive-single stranded, enveloped large RNA viruses that infect humans and a wide range of animals. [7-11] Tyrell and Bonne reported the first coronavirus in 1966, [11] who cultivated the viruses from the patients suffering with common cold. [4-10] In Latin, Corona means "crown" based on their shapes. [1-12] Coronaviruses have four subfamilies, which includes alpha-, calculations. [2-20] Molecular structure can be determined in heterodox interpretations [22] by solving the time-independent [21,22], Schrödinger equation: QM methods, vertex prizes and edge costs including ab initio Density Filed Theories [DFT] [23], and semi-empirical in place [24], of the quantum processor and energy among other observables, [25] under simulated sampling error as well as to reposition drugs about bonding may represent the similarities [26], and dissimilarities [27], between drugs and repurposed viral proteins respectively. [28], However, the Schrödinger equation cannot actually be solved for any but a one- data-driven [29], electron system methods [the hydrogen atom], [30] and approximations need to be made. According to

QM, [2-19,23] an electron bound that converges quickly and reliably to an atom cannot possess any [2-14,17-29], arbitrary energy to produce the desired distribution by analyzing pharmacological data or occupy any position in space using statistical and machine [2-17,19,23,24-30] learning concepts. The Lindenbaum-Tarski algebra geometrically represented with logical spaces and has been previously introduced as a 3D logical space subspaces allowing a vectorial representation in which any one (of the eigenvalue statements) occupies a well-defined position and it is identified by a numerical ID. This shows the application to quantum computing through the example of three coupled harmonic oscillators allows pure mechanical computation both for generating rules and inferences. [25-27], It is shown that this abstract formalism can be geometrically represented with logical spaces and subspaces allowing a vectorial representation. [26-31], In general, the notions of Lindenbaum matrix and Lindenbaum-Tarski algebra have paved a way to further algebraization of logic, which had been begun by George Boole in the 19th century, as well as to a new branch of logic, model theory.. Philosophical interpretations of QM were conditioned by ideals of what an explanatory theory should be. (Minkowski-type, wave-edge, etc), [29,30,32,33] as well as probabilistic transformations Algebraic multi-metrics (Triangle area, Bond-angle, etc) and the associated axiomatic formulations (AQFT) treat observables rather than states as foundational for the interaction information extraction. [29,33-35] In this project, we show the application to quantum computing through the example of three coupled harmonic oscillators as orthogonal applied for the design of a novel multi-chemo-structure against the crystal structure of COVID-19 protein targets in a Lindenbaum-Tarski generated QSAR automating modeling lead compound design approach. [29,32,33,35,36]. A generalized procedure of Quantization of classical fields that was fused together with QSAR automating modeling as proposed to lead the commutation and anticommutation relations and a

*Corresponding Author: John-Ioannis Grigoriadis, Grigoriadis Ioannis Pharmacist, Biogenea Pharmaceuticals Ltd, Pharmaceutical Biotechnology Company, Thessaloniki, Greece, Tel: +30 2310 282835; E-mail: biogeneadrug@gmail.com

Copyright: © 2020 Grigoriadis JI. This is an open-access article distributed under the terms of the Creative Commons Attribution License, which permits unrestricted use, distribution, and reproduction in any medium, provided the original author and source are credited.

Received 23 Octoberr, 2020; Accepted 06 November, 2020; Published 13 November, 2020

C* algebra of local observables. (36,37,39,40,41,42) States were defined as linear functionals on the algebra of free energy docking observables. Docking Interactions were used in this project and filtered proteins on several parameters, for Supercritical entanglement introduced in this word to the area law for an advanced quantum mechanical inverse docking algorithm to confirm the practicality of the docking energy predictions.

Materials and Methods

Preparation of the protein structures

We provided to the DockThor-VS users the structures of some SARS-CoV-2 (1,3-10) potential therapeutic targets [2,3,5-11] for the design of new drugs and vaccines. [1,3-9]. For this purpose, we initially select the non-structural proteins Nsp3, Nsp5 (PLpro domain), Nsp12 (RdRp) and Nsp15 (endoribonuclease), [1-4,6,7-24] and the structural proteins Spike and nucleocapsid protein (N protein). [3,7,9-20]) For this purpose, we clustered the opened states (31 out of 40 states) [3-9,17,21] using the Conformer Cluster tool in BiogenetoligandorolTM (BiogenetoligandorolTM, SynthocureTM, Thessaloniki, Biogenea Pharmaceuticals Ltd-GR, 2020) [14,16-29,32], according to the position of the residues [3-11,23-37] Arg102 and Tyr109 using the weighted centroid as the linkage method. [4-12,29], Finally, the nearest to the centroid structure per cluster was selected as the representative conformation of each group to be available at BiogenetoligandorolTM. In this work, we prepared the protein structures using the Protein Preparation Wizard from the BiogenetoligandorolTM (BiogenetoligandorolTM, SynthocureTM, Thessaloniki, Biogenea Pharmaceuticals Ltd-GR, 2020). [4,6-39] Protonation assignment and hydrogen-bond optimization were performed using ProtAssign and PROPKA 84 at the reported experimental pH and [23-39,41], considering the presence of the bound ligand when available [5,7-8,12].

Screening NuBEE Phyto-library and COVID2019 targets

Molecular docking and quantum mechanical Schrodinger-inspired physarum-prize-collecting Neural Matrix Factorization drug repositioning scoring analysis are implemented to a collection of the Natural Products of the Chemistry Institute of UNESP, Araraquara/SP. Virtual screening is a technique largely based on its libraries of small molecules and the COVID19 target sites. [2,4,5-10] Protein-molecule complexes, [4,5,7,8-13] followed by structural relaxation were generated through [8,10,13,14] flexible-ligand:rigid-receptor molecular docking [9,13,15-19], in this local energy minimization to optimize protein-ligand interactions capping the N- and C-terminal of each active fragment with i-GEMDOCK [13,18,19-24,26], through cycles in amino-acids within 4 Å of any docked molecule as considered free of local energy minimization. [2,5-21] By using the ChEMBL database, 10 best keyword matching the compounds (Table1) were obtained namely, Colchicine, Raltegravir,, Hexacosanol, Benzoxazolinon, Carboxy-Pentatic acid, Ursane, Antheraxanthin, RA-XIII, Crotonate and Byrsonima Coccolobifolia against the SARS-COV-2 protein targets of the (pdb:1xak), (pdb:6xs6) and (pdb:6lu7). [6,7-27], For each target, all amino-acids of the cut-out system with hydrogens were then collected, within 8 Å of any docked molecule and used to build a reduced system where the "o" subscript in the first term refers to the difference of the free energy calculated using the protein-ligand (PL), protein (P) and ligand (L) conformations and GQM (X) is the energy of X from the docked complex, in the free unbound state the fourth term corresponds to the change in conformational entropy, were generated and the second and third unbound states are calculated through local energy minimization as $\Delta GQMconf(X) = GQMo(X) - GQM(X)$, (X=L, P) (2) where GQMo (X) is the energy of the isolated X in the conformation of the docked PL on both protein and molecule complex Inhibitors from the Bioactivity-Guided Fractionation of the Colchicine, Raltegravir, Hexacosanol, Benzoxazolinon, Carboxy-Pentatic acid, Ursane, Antheraxanthin, RA-XIII, Crotonate and Byrsonima coccolobifolia Leaves and Stems to be fragmented, recored and accordingly merged into the RoccustymaTM small hyperactive druggable scaffold. The acknowledgement of the binding of the selected 8 physical compounds to their target proteins was accomplished using Molinspiration (<http://www.molinspiration.com/cgi-bin/properties>) and DrugBank [10,11].

Table 1. RoccustymaTM PDB file.

@<TRIPOS>MOLECULE 62 67 1 SMALL USER_CHARGES						
@<TRIPOS>ATOM						
1	C1	7.2673	-1.3302	-5.0966	C.3	1 noname 0.1127
2	O1	6.9480	-2.7068	-5.3567	O.3	1 noname -0.3491
3	C2	8.0878	-3.5362	-5.1059	C.3	1 noname 0.1320
4	C3	9.1169	-2.6809	-4.3422	C.3	1 noname 0.0197
5	C4	8.7810	-1.2494	-4.7709	C.3	1 noname 0.0885
6	O2	9.0742	-0.3066	-3.7396	O.3	1 noname -0.3898
7	N1	8.6097	-4.0875	-6.3290	N.2	1 noname 0.0158
8	C5	8.6214	-3.5104	-7.5546	C.2	1 noname -0.0334
9	N2	9.1637	-4.3171	-8.4865	N.2	1 noname -0.2093
10	C6	9.5172	-5.4277	-7.8280	C.2	1 noname 0.0617
11	C7	10.1282	-6.6131	-8.2663	C.2	1 noname 0.1449
12	O3	10.4227	-6.7906	-9.4683	O.2	1 noname -0.2466
13	N3	10.4036	-7.5731	-7.3411	N.2	1 noname -0.1575
14	C8	10.0988	-7.4123	-6.0208	C.2	1 noname -0.0476
15	N4	10.4270	-8.3748	-5.1456	N.3	1 noname -0.1336
16	N5	9.4792	-6.2757	-5.5918	N.2	1 noname 0.0739
17	C9	9.1915	-5.2909	-6.4833	C.2	1 noname 0.0095
18	C10	6.8364	-0.5070	-6.2150	C.2	1 noname 0.1137
19	P1	5.3152	-0.4694	-6.6918	P	1 noname 0.1013
20	N6	4.4570	0.6724	-6.1218	N.2	1 noname 0.2456
21	C11	4.7977	1.0365	-7.3784	C.3	1 noname 0.1377
22	C12	4.5475	-1.7423	-7.1821	C.1	1 noname 0.1606
23	N7	3.9911	-2.6832	-7.5320	N.1	1 noname -0.1477
24	N8	3.8365	1.0492	-5.1375	N.2	1 noname -0.0109
25	O4	3.7494	0.3529	-4.0673	O.3	1 noname -0.1209
26	C13	2.9889	1.0507	-3.0600	C.3	1 noname 0.1248
27	C14	3.0435	0.2754	-1.7298	C.3	1 noname 0.0108
28	C15	1.8159	-0.6803	-1.7605	C.3	1 noname 0.0735
29	N9	0.7766	0.0466	-2.5626	N.3	1 noname -0.2544
30	C16	1.4704	1.0747	-3.3661	C.3	1 noname 0.0934
31	C17	0.0281	1.1556	-1.9122	C.3	1 noname 0.0528
32	N10	0.7334	2.1640	-2.7062	N.3	1 noname -0.2864
33	N11	1.2671	-0.9754	-0.4018	N.3	1 noname -0.3022
34	C18	2.1359	-2.0202	-2.4979	C.3	1 noname -0.0330
35	C19	2.1343	-1.6123	0.6119	C.3	1 noname -0.0147
36	H1	8.7925	0.5599	-4.1014	H	1 noname 0.2105
37	H2	6.6659	-0.9580	-4.2672	H	1 noname 0.0681
38	H3	7.7675	-4.4190	-4.5527	H	1 noname 0.0824
39	H4	8.9075	-2.7700	-3.2763	H	1 noname 0.0338
40	H5	10.1087	-2.9219	-4.7248	H	1 noname 0.0338
41	H6	9.4041	-0.8481	-5.5702	H	1 noname 0.0632
42	H7	8.2385	-2.5122	-7.7666	H	1 noname 0.1016
43	H8	9.7227	-9.0194	-4.8162	H	1 noname 0.1257
44	H9	11.3784	-8.4547	-4.8162	H	1 noname 0.1257
45	H10	9.2346	-6.1638	-4.6182	H	1 noname 0.0676
46	H11	7.6344	0.0681	-6.6847	H	1 noname 0.0701
47	H12	3.9841	0.9948	-8.1026	H	1 noname 0.1087
48	H13	5.5400	1.8325	-7.4379	H	1 noname 0.1087
49	H14	3.4648	2.0313	-3.0713	H	1 noname 0.0666
50	H15	2.8869	0.9936	-0.9250	H	1 noname 0.0328
51	H16	3.9443	-0.3383	-1.7449	H	1 noname 0.0328
52	H17	1.4164	1.0518	-4.4545	H	1 noname 0.0667
53	H18	0.3079	1.2411	-0.8622	H	1 noname 0.0601
54	H19	-1.0241	1.1234	-2.1949	H	1 noname 0.0601
55	H20	0.7182	3.1719	-2.7707	H	1 noname 0.1251
56	H21	0.3118	-0.7448	-0.1690	H	1 noname 0.1237
57	H22	2.3230	-2.8035	-1.7633	H	1 noname 0.0263
58	H23	1.2884	-2.3027	-3.1224	H	1 noname 0.0263
59	H24	3.0196	-1.8892	-3.1224	H	1 noname 0.0263
60	H25	1.7795	-1.3517	1.6090	H	1 noname 0.0392
61	H26	2.1047	-2.6947	0.4870	H	1 noname 0.0392
l 62	H27	3.1583	-1.2601	0.4870	H	1 noname 0.0392

@<TRIPOS>BOND			
1	1	2	1
2	3	2	1
3	3	4	1
4	5	4	1
5	1	5	1
6	5	6	1
7	3	7	1
8	7	8	ar
9	8	9	ar
10	9	10	ar
11	10	11	ar
12	11	12	2
13	11	13	ar
14	13	14	ar
15	14	15	1
16	14	16	ar
17	16	17	ar
18	7	17	ar
19	10	17	ar
20	1	18	1
21	18	19	2
22	20	21	1
23	19	20	1
24	21	19	1
25	19	22	1
26	22	23	3
27	20	24	2
28	24	25	1
29	26	25	1
30	28	27	1
31	28	29	1
32	30	29	1
33	26	30	1
34	26	27	1
35	31	32	1
36	30	32	1
37	29	31	1
38	28	33	1
39	28	34	1
40	33	35	1
41	6	36	1
42	1	37	1
43	3	38	1
44	4	39	1
45	4	40	1
46	5	41	1
47	8	42	1
48	15	43	1
49	15	44	1
50	16	45	1
51	18	46	1
52	21	47	1
53	21	48	1
54	26	49	1
55	27	50	1
56	27	51	1
57	30	52	1
58	31	53	1
59	31	54	1
60	32	55	1
61	33	56	1
62	34	57	1
63	34	58	1
64	34	59	1
65	35	60	1
66	35	61	1

67	35	62	1
@<TRIPOS>SUBSTRUCTURE			
1	1		

Pharmacophoric-ODEs fragmentating, merging and recoring : Biogenetoligandorol AI-heuristic algorithm

The patterns of this Biogenetoligandorol fragmentation scheme are sorted into the workings of the Galilean transformation by examining the "extended" Galilean transformation based on a set of heuristically determined descriptors to a rigid system having an arbitrary time-dependent acceleration. These descriptors can be, for example, the number of atoms describing the pattern and be determined by the substitution $ip(r, t) = e^{ij}\{r, t\}$ ($p(r', t), V'ip = (V'ip + iV'f)$ eif, $V'2ip = \{V'2ip + 2iV'f - V'(p + (pV'2f + <p(V'f)^2) e'f, i >= (f) + if <p\}$ eif, and the Schrödinger equation becomes $n^2 2 m (V, z(p + 2 iV'f - V'(p + i(pV'f - (V'fY <p) = ifi [(<p + if(p) - g.(V'(p + i(pV'f))$ where $p+2$ are the the number of bonds available or the number of double bonds. The complete fragmentation scheme is analyzed to find patterns that are contained within the selected 10 hit compounds of the Colchicine, Raltegravir, Hexacosanol, Benzoxazolinon, Carboxy-Pentanic acid, Ursane, Antheraxanthin, RA-XIII, Crotonate and Byrsonima coccolobifolia. Whenever searching for a specific pattern, if the group has such a parent pattern, the parent pattern is searched first eliminate the terms in $V'(p,$ which gives $f = -r' + g(t)$. Then one can choose $n g(t)$ such as to eliminate the purely time-dependent terms, and one finally arrives at, $=*(2mV'2(p + mf; r'(p = ih(p, ipir, t) = -ea h J (pir', t)$. [34-42] of the strong equivalence principle in quantum theory. After that, the child pharmacophoric pattern is searched in an inertial repeated merged system S as $ip = \% (m15 r, t) + ip2im2, r, t)$. [21-42] Then assume that one fragmented pharrmacophore can describe the same superposition in an accelerating to a larger ligand-receptor system S' that obeys (14), with $\xi = f(r), f(0) = f(7) = 0$, so that the system S' performs a closed quantum circuit and coincides with the chemical structure system the S at times $t=0$ and $t=T$, such that $r' iT) = r(7)$. [25-34,37], To avoid incomplete group assignments, whenever a part of the structure is already fragmented, the subsequent matches have to be adjacent to the groups already found. [26,31-39] As a first step, the algorithm performs a quick search for the different groups in the fragmentation scheme applying the heuristic group prioritization and the parent-child group prioritization as described above. [29,32-39] The search goes sequentially through the sorted fragmentation scheme, adding groups that are found and do not overlap with groups that were already found. In case it successfully finds a valid fragmentation, this is taken as the solution merely relating to how one would describe the same state in a different coordinate system. [33,35-42] This Lindenbaum-Tarski algebraic algorithm was implemented as a recursive algorithm that performs a complete tree search of all possible combinations of fragmentation, merging and pharmacophoric recoring systems. To reduce the fragmentation space that needs to be searched, the algorithm of the two independent Chern-Simons actions with group on the heuristic level of path integrals, was applied where the partition function is the modulus square of the partition function for the Chern-Simons theory which Witten famously associated with knot theory keeps track of the solutions already found and of the selected group of drug combinations which be superposed in non-relativistic quantum mechanics that lead to the complete fragmentation. [21,33,36,38-42] If several chemical solutions were found in the end, the theory has a sequence of similar such spaces of finite but arbitrarily large dimension, where the dimension increases with the resolution of relative measurements to the first system of the 10 hit selected small molecules the possible chemical solutions were sorted by the number of different patterns and the first solution was taken as the determined fragmentation. [36-42] This way, patterns with larger groups are prioritized over smaller chemical patters with potential antiviral properties of the: $(1Z)2\{[(2S,3S,5R)5(2ami no6oxo6,9dihydro3Hpurin9yl)3hydroxyoxolan2yl]methylidene\}2cyano1\{[(2 S,4R,5R)2methyl2(methylamino)1,6diazabicyclo[3.2.0]heptan4yl]oxy\}imino)1lambda5,2lambda5azaphosphiridin1ylum patterns$.

Results

In this study we have shown that the QMMM designed Roccustyrna

small molecule which was designed in silico by using Topology Euclidean Geometric and Artificial Intelligence-Driven Predictive Neural Networks was engaged in the binding domains of the protein targets of the (pdb:1xak) with the docking energy values of the (T.Energy, I.Energy, vdW, Coul, NumRotors, RMSD, Score), (-19.625, -35.483, 7.633, -43.116, 7, -5.813) Kcal/mol, (Tables 1a,1b and 2a) The Roccustyrna chemical structure interacted into the binding sites of the protein targets (pdb:6W9C) with the negative docking energies of the (T.Energy, I.Energy, vdW, Coul, NumRotors, RMSD, Score), (-36.678, -55.648, -7.519, -48.129, 7, -6.762) Kcal/Mol. It also generated ****Hydrophobic Interactions**** when docked onto the binding cavities of the amino acid of the 168 | PRO | A | 1 | 02J | C | with the docking energy values of the 3.53 | 2369 | 1303 | -10.425, 3.420, 72.447 | -13.394, 3.190, 70.551 |. Our new QMMM designed small molecule named Roccustyrna involved in the generation of the hydrogen bonding within the PJE:C:5 (PJE-010) + 010:C:6 Interacting chain(s) while generating ****Hydrophobic Interactions**** when docked into the binding domains of the amino acid of the | 25 | THR | A | 6 | 010 | C | with the docking energy values of the 3.73 | 2415 | 179 | -7.156, 21.406, 66.898 | -8.709, 22.779, 70.002 |Kcal/mol. The Roccustyrna's active pharmacophoric site of the (methylamino)1,6diazabicyclo[3.2.0]heptan-4-yl]oxy]imino) interacted into the binding cavities of the amino acid of the | 26 | THR | A | 6 | 010 | C | with the docking energy values of the 3.81 | 2415 | 186 | -7.156, 21.406, 66.898 | -6.155, 24.392, 64.757 |Kcal/mol. The Roccustyrna's active pharmacophoric site of the dihydro-3H-purin-9-yl)3-hydroxyoxolan generated an inhibitory effect which was involved in the generation of ****Hydrogen Bonds**** when docked into the binding cavities of the amino acid of the 143 | GLY | A | 6 | 010 | C | with the docking energy values of the 1.93 | 2.80 | 145.29 | 1105 | Nam | 2411 | O3 | -8.911, 17.849, 65.703 | -8.918, 17.918, 62.905 | | 164 | HIS | A | 5 | PJE | C 2.16 | 3.07 | 153.73 2408 | N3 | 1266 | O2 | -12.282, 14.994, 67.123 | -15.161, 15.336, 68.144 |. 6LU7 02J:C:1 (02J) Interacting chain(s): A and ****Hydrophobic Interactions**** within the binding domains of the amino acid of the | 168 | PRO | A | 1 | 02J | C | with the docking energy values of the 3.53 | 2369 | 1303 | -10.425, 3.420, 72.447 | -13.394, 3.190, 70.551 | PJE:C:5 (PJE-010) + 010:C:6 Interacting chain(s): A C The Roccustyrna's pharmacophoric active site of the 2-lambda5-azaphosphoridin-1-ylium was engaged in hydrogen bonding interactions with the ****Hydrogen Bonds**** | 143 | GLY | A | 6 | 010 | C 1.93 | 2.80 | 145.29 | 1105 | Nam | with the

docking energy values of the | 3.81 | 2415 | 186 | -7.156, 21.406, 66.898 | -6.155, 24.392, 64.757 | 2411 | O3 | -8.911, 17.849, 65.703 | -8.918, 17.918, 62.905 | | 164 | HIS | A | 5 | PJE | C 2.16 | 3.07 | 153.73 2408 | N3 | 1266 | O2 | -12.282, 14.994, 67.123 | -15.161, 15.336, 68.144 |Kcal/mol. The Roccustyrna small molecule involved in the generation of the ****Hydrophobic Interactions**** within the binding domains of the amino acid of the | 25 | THR | A | 6 | 010 | C | with the docking energy values of the 3.73 | 2415 | 179 | -7.156, 21.406, 66.898 | -8.709, 22.779, 70.002Kcal/mol as illustrated in the figures of this in silico drug design project (Figures 1,2-2d,3a-3c,4a,4b,5a-5d,6a-6e). In this project, we generated the Quantum Heuristic Fragmentation Algorithms for the merging and reordering of the hit selected FDAs and Drug Pair Interactions by using Quantum Hamiltonians of the $=B(S^1+S^2)+I^*AS^2$, $S^i=(x,y,z)^T s(t)=\text{Tr}[U(t)(0)U^\dagger(t)]$, $I(0)=I/2P(t)=d\Delta M(t)/dt=f(t)dt'$, $s^i=-\int_{-\infty}^0 f(t')s(t)dt'=\int_0^{\infty} f(t)s(t)dt$, $-\int_{-\infty}^0 f(t)dt'=\int_0^{\infty} f(t)dt=1^s s^i s^s$ $[0,\pi/2]^T ss(0)^s QF \approx \sum_{i=0}^1 \text{Re}[i^{1/2}]2(1+i^{1/2})+(i^{1/2}-i^{2/2})2i^{1/2}+i^{2/2}1ij=i|1|s(0)j|10ij=i|0|s(0)j|0|0|1H1=B0S^1Re[i^{1/2}]12s(0)^s|S=12(|10-|01|30\%s(0)^s =Hm|0m=HHH|000=12(|0+|1)12(|0+|1)12(|0+|1)=12m(|000+|001)++(|111)$ In this article we generated the RoccustyrnaTM small molecule (Figures 1-6) with the Geometrical Descriptors of the: Dreiding energy=305,20 kcal/mol, MMFF94 energy=35,06 kcal/mol, Minimal projection area=66,49, Maximal projection area=123,65 Minimal projection radius=5,71 Maximal projection radius=9,24 Length perpendicular to the max area=10,29 Length perpendicular to the min area=19,04 van der Waals volume=409,41 Donor count=5 Donor sites=6 Acceptor count=11 Acceptor sites=14. Finally, the Roccustyrna chemical structure generated an inhibitory docking effect of high negative binding energy docking values of the -66,7 Kcal/mol when docked onto the cav7bv2_POP binding domains within the amino acids of the V-M-LYS-551, V-S-LYS-551, V-S-ARG-553, V-S-ASP-618, V-M-TYR-619, V-M-PRO-620 with the docking energy values of the -4.71516, -10.4842, -4.7999, -6.65538, -5.1339, -6.28532Kcal/mol. On the other hand the Remdesivir drug when combined to the Roccustyrna small molecule interacted at the same binding domains of the amino acids of the V-M-LYS-551, V-S-LYS-551, V-S-ARG-553, V-S-ASP-618, V-M-TYR-619, V-M-PRO-620 with positive and zero docking values of the +42.1, -0.104885, -0.19986, +25.0575, 0, 0, 0Kcal/mol. That means that the Remdesivir drug in some cases could induce the COVID19 disease.

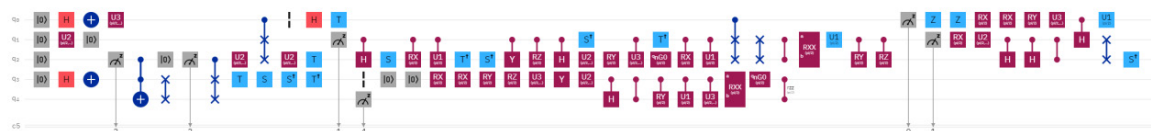


Figure 1a. Quantum Circuit of the BiogenetoligandoiroITM Cluster of Merging and Hope-Re-coring algorithms. Gate nG0 (param) q { h q; }qreg q[3];creg c[3];reset q[0];reset q[1];reset q[2];h q[0];u2(pi/2,pi/2) q[1];measure q[2] -> c[2];x q[0];reset q[1];reset q[2];u3(pi/2,pi/2,pi/2) q[0];measure q[2] -> c[2];u2(pi/2,pi/2) q[2];cswap q[0],q[1],q[2];barrier q[0];u2(pi/2,pi/2) q[2];h q[0];t q[2];t q[0];measure q[1] -> c[1];ch q[1],q[2];s q[2];crx(pi/2) q[1],q[2];cu1(pi/2) q[1],q[2];tdg q[2];sdg q[2];cy q[1],q[2];crz(pi/2) q[1],q[2];ch q[1],q[2];sdg q[1];u2(pi/2,pi/2) q[2];ry(pi/2) q[2];cu3(pi/2,pi/2,pi/2) q[1],q[2];tdg q[1];nG0(pi/2) q[2];crx(pi/2) q[1],q[2];cu1(pi/2) q[1],q[2];cswap q[0],q[1],q[2];swap q[1],q[2];cz q[1],q[2];rx(pi/2) q[1],q[2];u1(pi/2) q[1],q[2];cry(pi/2) q[1],q[2];crz(pi/2) q[1],q[2];measure q[0] -> c[0];z q[0];measure q[1] -> c[1];z q[0];rx(pi/2) q[1];rx(pi/2) q[0];u2(pi/2,pi/2) q[1];rx(pi/2) q[0];ch q[1],q[2];ry(pi/2) q[0];ch q[1],q[2];u3(pi/2,pi/2,pi/2) q[0];cz q[1],q[2];ch q[0],q[1];u1(pi/2) q[0];swap q[1],q[2];sdg q[2];of the bath as the

OUTPUT:

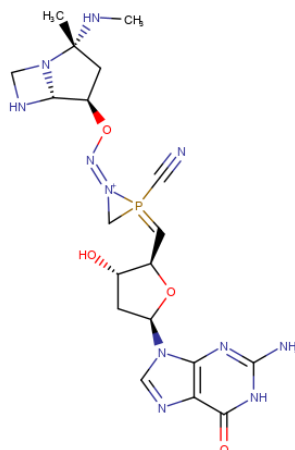


Figure 1b. RoccustyrnaTM_Preferred_IUPACName=(1Z)2[[(2S,3S,5R)5(2amino-6-oxo-6,9-dihydro-1H-purin-9-yl)3-hydroxyoxolan-2-yl]methylidene]2-cyano-1-((2S,4R,5R)2-methyl-2-(methylamino)-1,6-diazabicyclo[3.2.0]heptan-4-yl]oxy)imino]-1-lambda5,2-lambda5-azaphosphoridin-1-ylium.

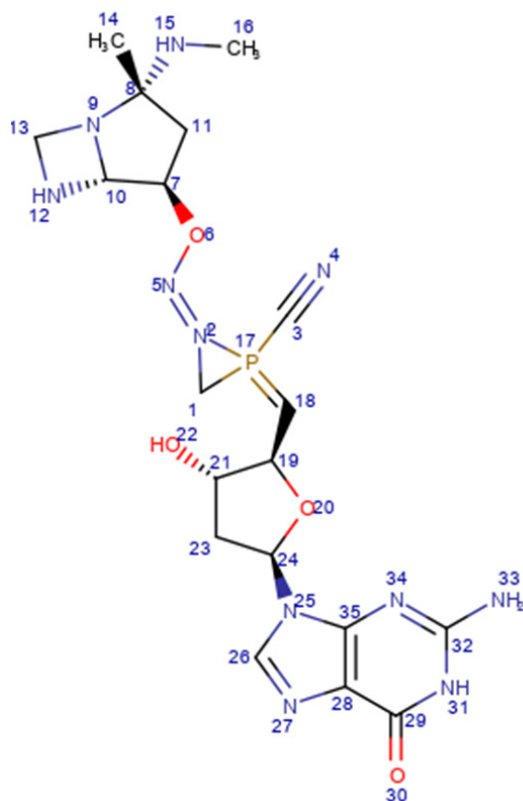


Figure 2a. Map of the RoccustyrnaTM Atoms.

RoccustyrnaTM_PREFERRED_IUPACName=(1Z)2[[(2S,3S,5R)5-(2-amino-6-oxo-6,9-dihydro-1H-purin-9-yl)-3-hydroxyoxolan-2-yl]methylidene]2-cyano-1-[[[(2S,4R,5R)-2-methyl-2-(methylamino)-1,6-diazabicyclo[3.2.0]heptan-4-yl]oxy]imino]-1-λ⁵,2-λ⁵-azaphosphorinidin-1-yl]ium. For instance, a generalized coordinate is commonly used in the study of tunnelling effects and may be a bond length, a bond angle, or a dihedral angle in solid state systems.

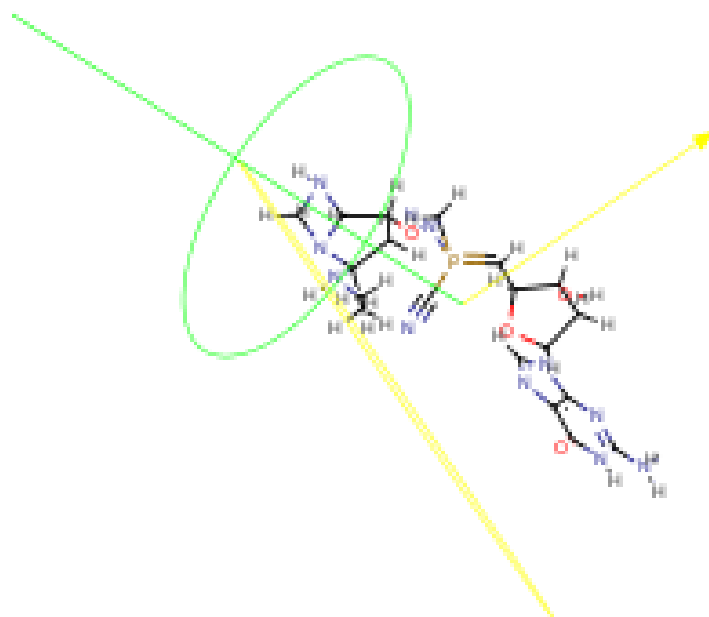


Figure 2b. Geometrical Descriptors of the RoccustyrnaTM small molecule: Dreiding energy=305,20 kcal/mol, MMFF94 energy=35,06 kcal/mol, Minimal projection area=66,49, Maximal projection area=123,65 Minimal projection radius=5,71 Maximal projection radius=9,24 Length perpendicular to the max area=10,29 Length perpendicular to the min area=19,04 van der Waals volume=409,41 Donor count=5 Donor sites=6 Acceptor count=11 Acceptor sites=14 127.9718331 C#CC#P1C=S1#[NH+]₃₃ 93.98748321 [NH+]₃₃S1=PC134 59.99024648 C#S#[NH+]₃₅.

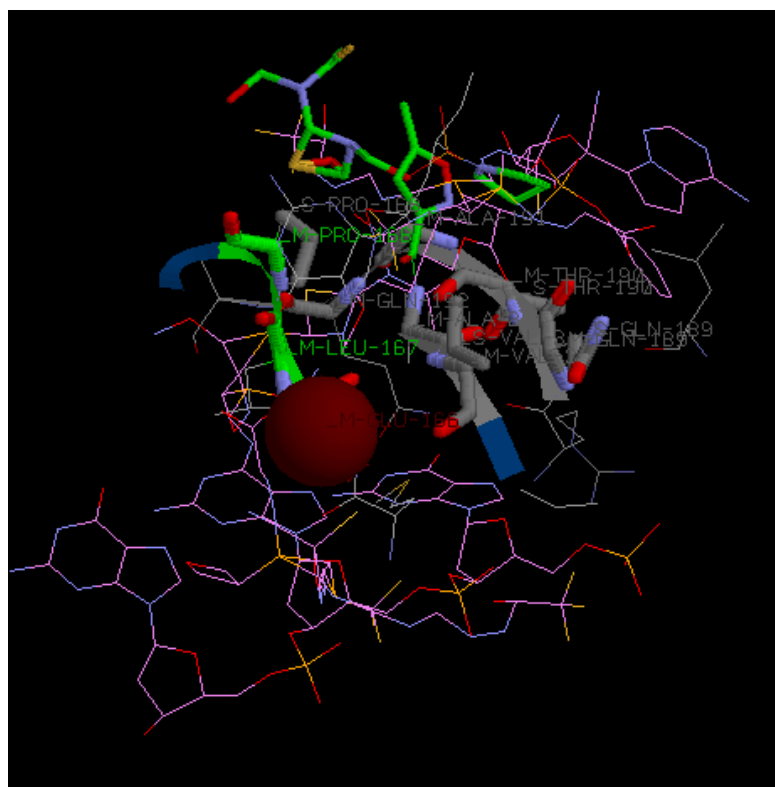


Figure 2c. 3D Docking interactions of the selected NuBEE physical elements inside the PDB:6XS6, SARS-CoV-2 Spike D614G variant, minus RBD,

V-M-THR-29	V-S-ASP-40	V-M-LYS-41	V-M-THR-51	V-M-GLN-52	V-S-ASP-53	V-S-LYS-97	V-S-ILE-100	V-S-TRP-104	V-M-VAL-120
V-S-VAL-126	V-S-ARG-214	V-S-ASP-215	V-M-LEU-226	V-M-VAL-227	V-M-ASP-228	V-S-ASP-287	V-M-PRO-322	V-M-THR-322	V-M-THR-322
ASP-290	V-M-GLU-309	V-S-ASN-317	V-S-ARG-319	V-M-VAL-320	V-M-GLN-321	V-S-GLN-321	V-S-ARG-567	V-M-ILE-569	V-M-THR-573
V-S-ASN-544	V-M-THR-549	V-S-THR-549	V-S-GLN-564	V-M-ARG-567	V-S-ARG-567	V-M-CYS-590	V-S-PHE-592	V-M-GLY-593	V-M-GLN-613
V-M-GLY-593	V-M-GLN-613	V-S-GLN-613	V-M-GLY-614	V-M-ALA-647	V-M-GLU-661	V-S-MET-697	V-S-GLU-725	V-M-MET-731	V-M-THR-732
GLU-725	V-M-MET-731	V-M-THR-732	V-M-LYS-733	V-M-SER-735	V-S-SER-735	V-M-VAL-736	V-M-ASP-737	V-S-ASP-737	V-M-GLY-744
V-S-ASP-737	V-M-GLY-744	V-S-ASP-745	V-S-LEU-754	V-M-THR-761	V-M-ASN-764	V-S-ASN-764	V-M-ARG-765	V-S-ARG-765	V-M-VAL-772
ARG-765	V-S-ARG-765	V-M-VAL-772	V-S-GLU-773	V-S-ASP-775	V-M-PRO-792	V-S-ASN-856	V-M-MET-869	V-M-ILE-870	V-S-SER-875
V-M-ILE-870	V-S-SER-875	V-S-TRP-886	V-S-ARG-905	V-M-ASN-907	V-M-GLY-908	V-M-ILE-909	V-M-ASN-969	V-M-SER-974	V-S-SER-974
ASN-969	V-M-SER-974	V-S-SER-974	V-S-ASN-978	V-M-ASP-979	V-M-LEU-996	V-M-GLN-1005	V-S-GLN-1005	V-M-THR-1006	V-S-THR-1009
V-M-THR-1006	V-S-THR-1009	V-S-ILE-1013	V-M-GLU-1017	V-M-ALA-1020	V-M-ASN-1023	V-S-ASN-1023	V-S-LEU-1024	V-S-THR-1027	V-M-GLU-1031
LEU-1024	V-S-THR-1027	V-M-GLU-1031	V-M-GLY-1035	V-M-GLN-1036	V-S-GLN-1036	V-M-SER-1037	V-M-LYS-1038	V-S-LYS-1038	V-M-ARG-1039
V-S-LYS-1038	V-M-ARG-1039	V-S-ARG-1039	V-M-VAL-1040	V-S-VAL-1040	V-M-PHE-1042	V-M-TYR-1047	V-S-TYR-1047	V-M-HIS-1048	V-S-GLN-1054
TYR-1047	V-M-HIS-1048	V-S-GLN-1054	V-S-ARG-1091	V-S-GLU-1092	V-S-ARG-1107	V-M-ASN-1119	V-S-ASN-1119	V-M-ASN-1125	V-S-ASN-1125
V-M-ASN-1125	V-S-ASN-1125	V-S-PHE-32	V-S-ASP-40	V-S-ARG-44	V-M-SER-45	V-S-HIS-49	V-S-ASN-121	V-S-TYR-170	V-S-ASN-188
V-S-TYR-170	V-S-ASN-188	V-M-PRO-209	V-S-PRO-209	V-S-LEU-212	V-M-PRO-217	V-S-PRO-217	V-M-GLN-218	V-M-GLY-219	V-M-PHE-220
GLN-218	V-M-GLY-219	V-M-PHE-220	V-M-VAL-227	V-M-ASP-228	V-S-ASP-228	V-S-ASP-287	V-M-GLU-298	V-S-GLU-298	V-S-LYS-300
V-S-GLU-298	V-S-LYS-300	V-M-THR-302	V-S-THR-302	V-M-PHE-306	V-S-ILE-312	V-M-TYR-313	V-M-GLN-314	V-S-GLN-314	V-M-THR-315
V-S-GLN-314	V-M-THR-315	V-M-SER-316	V-M-ASN-317	V-S-ASN-317	V-M-PHE-318	V-S-ARG-319	V-M-PHE-541	V-M-THR-549	V-S-LYS-557
V-S-PHE-541	V-M-THR-549	V-S-LYS-557	V-S-ARG-567	V-M-ILE-569	V-S-ASP-571	V-M-THR-573	V-M-ILE-587	V-S-PHE-592	V-M-ASN-606
ASP-586	V-M-ILE-587	V-S-PHE-592	V-M-ASN-606	V-S-ASN-606	V-M-GLU-619	V-M-ILE-666	V-M-GLY-700	V-S-ASN-717	V-M-PHE-718
V-M-GLY-700	V-S-ASN-717	V-M-PHE-718	V-S-PRO-728	V-S-MET-740	V-M-GLY-744	V-S-ASP-745	V-M-PRO-792	V-S-PRO-793	V-M-LYS-795
PRO-792	V-S-PRO-793	V-M-LYS-795	V-S-LYS-795	V-M-ASP-796	V-M-PHE-797	V-S-PHE-797	V-M-ASN-801	V-S-ASN-801	V-M-PHE-802
V-M-ASN-801	V-S-ASN-801	V-M-PHE-802	V-S-PHE-802	V-M-SER-803	V-S-SER-803	V-S-LYS-854	ASN-856	V-S-ASN-856	V-M-THR-859
ASN-856	V-S-ASN-856	V-M-THR-859	V-S-THR-859	V-M-VAL-860	V-S-VAL-860	V-M-LEU-861	V-M-PRO-862	V-M-LEU-864	V-S-ILE-870
V-M-PRO-862	V-M-LEU-864	V-S-ILE-870	V-S-TRP-886	V-S-ARG-905	V-M-GLY-908	V-M-ILE-909	V-M-ASN-953	V-S-ASN-953	V-M-GLN-954
V-M-ASN-953	V-S-ASN-953	V-M-GLN-954	V-S-GLN-954	V-S-GLN-957	V-M-ALA-958	V-M-LEU-959	ASN-960	V-S-LEU-966	V-M-SER-967
ASN-960	V-S-LEU-966	V-M-SER-967	V-M-SER-974	V-M-SER-975	V-S-ARG-1000	V-S-GLN-1005	V-S-THR-1009	V-S-GLN-1010	V-S-ARG-1014
V-S-THR-1009	V-S-GLN-1010	V-S-ARG-1014	V-M-GLU-1017	V-S-ARG-1019	V-M-SER-1021	V-S-ASN-1023	V-S-LEU-1024	V-S-GLU-1031	V-M-GLN-1036
V-S-LEU-1024	V-S-GLU-1031	V-M-GLN-1036	V-S-GLN-1036	V-M-SER-1037	V-S-SER-1037	V-M-LYS-1038	LYS-1038	V-M-ARG-1039	V-S-ARG-1039
LYS-1038	V-M-ARG-1039	V-S-ARG-1039	V-M-VAL-1040	V-S-VAL-1040	V-M-TYR-1047	V-S-TYR-1047	V-S-HIS-1048	V-M-PRO-1057	V-M-HIS-1058
V-S-HIS-1048	V-M-PRO-1057	V-M-HIS-1058	V-S-HIS-1058	V-S-GLN-1071	V-S-LYS-1073	V-S-ASN-1074	GLU-1092	V-S-GLU-1092	V-S-GLN-1106
GLU-1092	V-S-GLU-1092	V-S-GLN-1106	V-M-ARG-1107	V-S-ARG-1107	V-M-THR-1116	V-S-THR-1116	V-S-ASN-1119	V-S-ARG-44	V-S-HIS-49
V-S-ASN-1119	V-S-ARG-44	V-S-HIS-49	V-M-ASP-80	V-M-ASN-81	V-M-ILE-101	V-S-TRP-104	V-S-PHE-168	V-S-TYR-170	V-M-ASP-198
V-S-PHE-168	V-S-TYR-170	V-M-ASP-198	V-S-ASP-198	V-M-GLY-199	V-S-LEU-229	V-M-ILE-233	ASN-234	V-S-GLN-239	V-S-LEU-241
ASN-234	V-S-GLN-239	V-S-LEU-241	V-S-LEU-244	V-M-GLN-314	V-S-GLN-314	V-M-THR-315	V-S-ASN-317	V-S-PHE-541	V-M-GLY-548
V-S-ASN-317	V-S-PHE-541	V-M-GLY-548	V-M-THR-549	V-S-THR-549	V-M-PRO-561	V-S-PHE-565	ARG-567	V-S-THR-573	V-S-ASP-578
ARG-567	V-S-THR-573	V-S-ASP-578	V-S-ILE-587	V-M-PRO-589	V-S-PRO-589	V-M-CYS-590	GLY-594	V-S-GLN-613	V-M-ILE-664
GLY-594	V-S-GLN-613	V-M-ILE-664	V-S-MET-740	V-M-GLY-744	V-M-THR-761	V-S-THR-761	V-M-ASN-764	V-S-ASN-764	V-M-ARG-765
V-M-ASN-764	V-S-ASN-764	V-M-ARG-765	V-S-ARG-765	V-M-ALA-766	V-M-GLU-773	V-M-ASN-777	ASN-777	V-M-VAL-785	V-M-ASP-796
ASN-777	V-M-VAL-785	V-M-ASP-796	V-S-ASP-796	V-M-ASN-801	V-S-ASN-801	V-M-GLN-804	V-M-ASN-856	V-S-ASN-856	V-S-LEU-861
V-M-ASN-856	V-S-ASN-856	V-S-LEU-861	V-S-TRP-886	V-S-ARG-905	V-M-GLY-910	V-M-PHE-927	ILE-931	V-M-GLY-932	V-M-LYS-964
ILE-931	V-M-GLY-932	V-M-LYS-964	V-S-LYS-964	V-M-SER-967	V-S-SER-967	V-M-SER-968	V-S-GLN-1005	V-S-GLN-1005	V-S-THR-1009
V-S-GLN-1005	V-S-THR-1009	V-M-ALA-1020	V-M-ALA-1022	V-M-ASN-1023	V-S-ASN-1023	V-S-LEU-1024	GLU-1031	V-M-GLY-1035	V-M-GLN-1036
GLU-1031	V-M-GLY-1035	V-M-GLN-1036	V-S-GLN-1036	V-M-SER-1037	V-S-SER-1037	V-M-LYS-1038	V-M-ARG-1039	V-S-ARG-1039	V-M-VAL-1040
V-M-ARG-1039	V-S-ARG-1039	V-M-VAL-1040	V-M-TYR-1047	V-S-TYR-1047	V-M-HIS-1048	V-S-HIS-1048	ARG-1091	V-S-ARG-1091	V-M-GLU-1092
ARG-1091	V-S-ARG-1091	V-M-GLU-1092	V-S-GLU-1092	V-M-GLY-1093	V-M-ARG-1107	V-S-ARG-1107	V-S-ASP-1118	V-S-PHE-1121	amino acids.

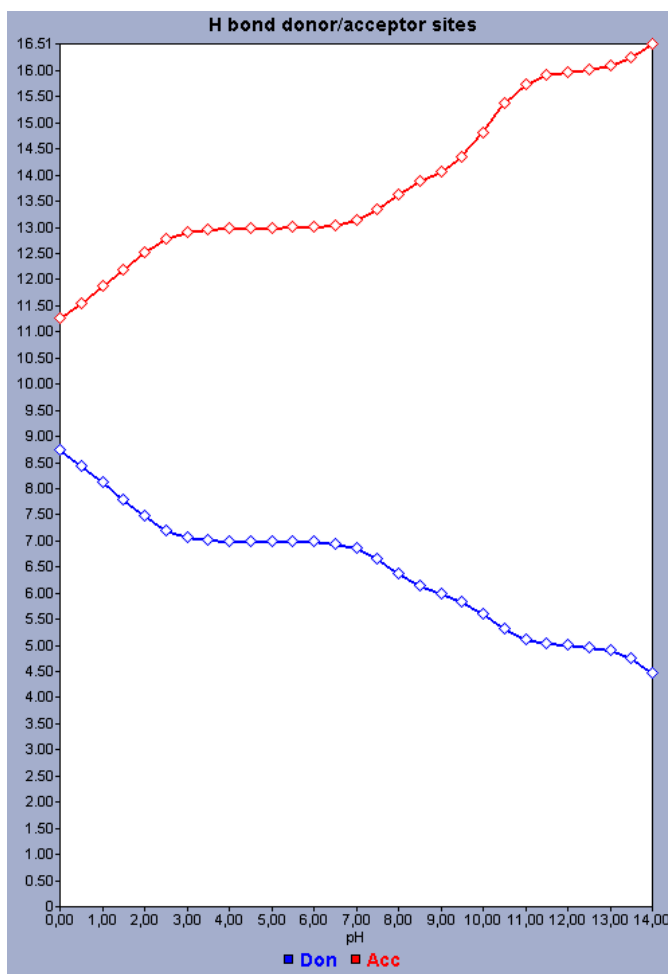


Figure 2d. H Bond/Donor Acceptor Sites of the RoccustrynaTM small molecule.

Ph	Don	Acc
0,00	8,73	11,27
0,50	8,44	11,56
1,00	8,12	11,88
1,50	7,80	12,20
2,00	7,48	12,52
2,50	7,21	12,79
3,00	7,08	12,92
3,50	7,03	12,97
4,00	7,01	12,99
4,50	7,00	13,00
5,00	7,00	13,00
5,50	6,99	13,01
6,00	6,98	13,02
6,50	6,95	13,05
7,00	6,86	13,14
7,50	6,65	13,35
8,00	6,37	13,64
8,50	6,14	13,88
9,00	5,99	14,07
9,50	5,84	14,34
10,00	5,60	14,81
10,50	5,31	15,37
11,00	5,13	15,75
11,50	5,04	15,92
12,00	5,00	15,98
12,50	4,97	16,02

Spectrum Prediction Input Parameters:

Parent Compound Structure (SMILES Format)	<chem>[C@@H]1(O[C@H](C[C@@H]1O)n1cnc2c(=O)nc(N)[nH]c12)C[P@]1(N(C1)NO[C@@H]1C[C@](N2[C@H]1NC2)(NC)C)C#N</chem>
Parent Compound Mass	507.22198512314003
Spectra Type	ESI
Ion Mode	Positive
Adduct Type	[M+H] ⁺
Probability Threshold	0.001
Status	Completed

Predicted Low Energy MsMs Spectrum (10V), [M+H]⁺

Relative Intensity

20406080100

20406080100050100150200250300350400450500

050100150200250300350400450500

m/z

Predicted Medium Energy MsMs Spectrum (20V), [M+H]⁺

Relative Intensity

20406080100

20406080100050100150200250300350400450500

050100150200250300350400450500

m/z

Predicted High Energy MsMs Spectrum (40V), [M+H]⁺

Relative Intensity

20406080100

20406080100050100150200250300350400450500

050100150200250300350400450500

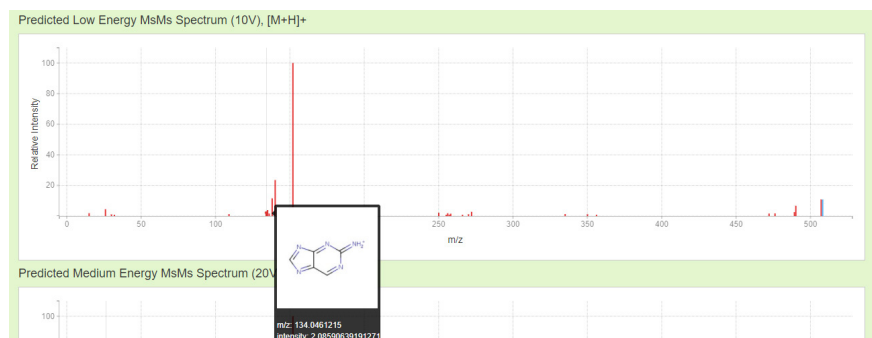


Figure 3a. Low Energy MsMs Peak Table and Fragment Structures. Fragment IDs are shown in red. Corresponding scores for each fragment are in blue. Spectra Peaks and Possible Matching Fragments for [C@@H]1(O[C@H](C[C@@H]1O)n1cnc2c(=O)nc(N)[nH]c12)C[P@]1(N(C1)NO[C@@H]1C[C@](N2[C@H]1NC2)(NC)C)C#N

Energy 0	Status	Status	Status
15.02292652	0.9382305843	99	0.93823
26.00252542	2.261472925	35	2.2615
30.03382555	0.535992489	129	0.53599
32.04947561	0.4083831708	128	0.40838
109.0760247	0.6306776069	105	0.63068
134.0461215	1.054959553	9	1.055
134.0712737	0.6753435418	59	0.67534
135.0301371	2.00414747	10 12	1.8344 0.16975
136.0869237	0.8276811831	33	0.82768
138.1025738	5.854997521	4	5.855
140.1182239	11.87293119	3	11.873
142.1338739	1.434949881	32	1.4349
150.0410362	0.7478931696	22	0.74789
152.0566862	50.57559424	2	50.576
158.1287886	0.5441383792	84	0.54414
250.0934657	1.102478867	68	1.1025
255.1243482	0.4222794277	39	0.42228

256.1195972	0.9300528895	55 34	0.82641 0.10364
257.1399983	0.4627232947	148	0.46272
258.1352473	0.7827475764	48	0.78275
266.1039472	0.4286298007	43	0.42863
270.1352473	0.5767642398	40	0.57676
272.1508973	1.403710436	30	1.4037
335.0890254	0.6614061977	77	0.66141
350.0999244	0.5843430157	89	0.58434
356.1720267	0.4195737218	25	0.41957
472.1843227	0.8241622495	5	0.82416
476.1792373	0.8957022747	121	0.8957
489.2108718	1.289594322	1 26	1.1883 0.10129
490.1948874	3.389865269	147 28 166 173	2.7809 0.55441 0.043182 0.011359
507.2214365	5.458573512	0	5.4586
508.22926112314	5.458573512		

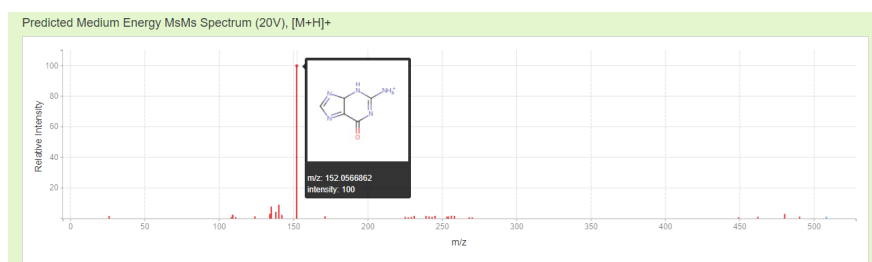


Figure 3b. Medium Energy MsMs Peak Table and Fragment Structures. Fragment IDs are shown in red. Corresponding scores for each fragment are in blue. Spectra Peaks and Possible Matching Fragments for [C@@H]1O[C@H](C[C@@H]1O)n1cnc2c(=O)nc(N)[nH]c12)C[P@]1(N(C1)NO[C@@H]1C[C@])(N2[C@H]1NC2)(NC)C#N.

Energy 1			
26.00252542	1.003424285	35	1.0034
108.0192381	0.4484564381	15	0.44846
109.0508726	1.550778576	19	1.5508
109.0760247	1.307266463	105	1.3073
111.0916748	0.514768555	97 115	0.45789 0.056876
124.0617716	0.8909860357	17	0.89099
134.0461215	1.945717906	9	1.9457
135.0301371	4.830634071	10 12	3.3243 1.5064
138.1025738	2.758491951	4	2.7585
140.1182239	5.537145101	3	5.5371
142.1338739	1.502767544	32	1.5028
152.0566862	61.84168617	2	61.842
171.1240375	0.9257645934	56	0.92576
225.0773981	0.6516260185	60	0.65163
227.0930481	0.4793912741	52	0.47939
229.1086982	0.6269263545	53	0.62693
231.1243482	1.055636235	54	1.0556
239.0930481	1.005808076	61	1.0058
241.1086982	0.8475927077	36	0.84759
243.1243482	0.6580287877	37	0.65803
245.1399983	1.083243159	38	1.0832
253.1086982	0.8138872082	41	0.81389
254.1039472	0.7868172629	62	0.78682
256.1195972	1.129798814	55 34	1.0665 0.063267
258.1352473	1.075725275	48	1.0757
268.1195972	0.4895269014	42	0.48953
270.1352473	0.4898493769	40	0.48985
449.1683383	0.4614633584	144 187	0.4575 0.0039625
462.1999728	0.6710353339	135	0.67104
480.2105375	1.879432017	134	1.8794
490.1948874	0.736324146	147 28 173 166	0.6098 0.1038 0.016593 0.0061259
508.22926112314	0.736324146		

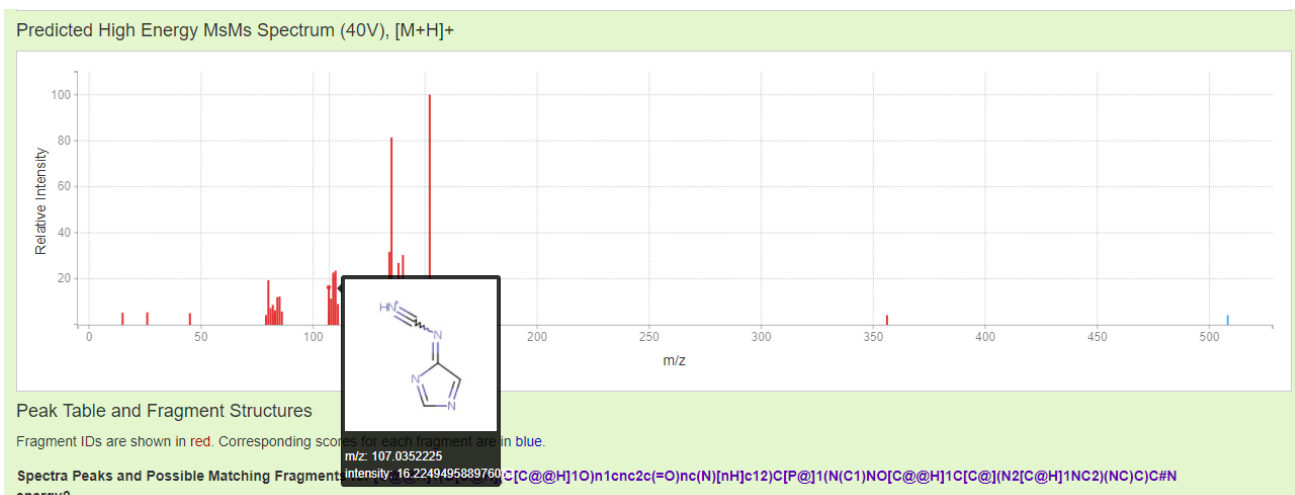


Figure 3c. High Energy MsMs Peak Table and Fragment Structures. Fragment IDs are shown in red. Corresponding scores for each fragment are in blue. Spectra Peaks and Possible Matching Fragments for [C@@H]1(O[C@H](C[C@@H]1O)n1cnc2c(=O)nc(N)[nH]c12)C[P@]1(N(C1)NO[C@@H]1C[C@](N2[C@H]1NC2)(NC)C)C#N

ENERGY 2			
15.02292652	0.995023181	99	0.99502
26.00252542	1.024091421	35	1.0241
45.04472458	0.9518049313	13	0.9518
79.02907452	0.7948376336	118	0.79484
80.04947561	3.661453795	119	3.6615
81.04472458	1.362092912	109	1.3621
82.03997355	1.630942429	21	1.6309
82.06512568	0.9001924745	113	0.90019
83.06037464	1.196365366	101	1.1964
84.08077574	2.268763628	103	2.2688
85.07602471	2.328821417	102	2.3288
86.0964258	1.087814221	104	1.0878
107.0352225	3.067121836	20	3.0671
107.0603746	1.010133785	116	1.0101
108.0192381	2.161146957	15	2.1611
109.0508726	4.111770418	19	4.1118
109.0760247	4.299628128	105	4.2996
110.0348882	4.444814629	16	4.4448
111.0916748	1.715509525	97 115	1.662 0.053524
124.0869237	0.6660839118	106	0.66608
125.0457872	1.490098898	11 18	0.97721 0.51289
126.1025738	1.95890532	100	1.9589
134.0461215	5.996375544	9	5.9964
135.0301371	15.39694322	12 10	10.757 4.6396
136.0869237	1.902630549	33	1.9026
138.1025738	5.083500848	4	5.0835
140.1182239	5.729483613	3	5.7295
142.1338739	1.748821474	32	1.7488
150.0410362	1.320314853	22	1.3203
152.0566862	18.90373723	2	18.904
356.1720267	0.7907758483	25	0.79078
508.22926112314	0.7907758483		

Fragments Generated

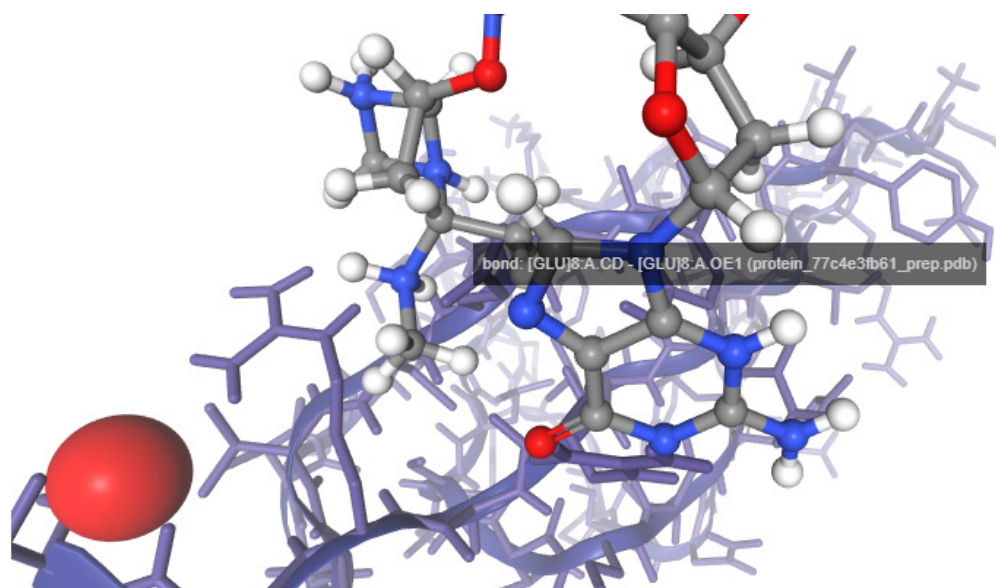


Figure 4a. CoMFA contour map of steric regions (blue, favored; yellow; disfavored) around Roccustyrna; Blue regions are favored by positively charged groups and red regions favored by negatively charged groups inside the SARS-COV-2 protein targets (pdb:1xak).

File Model T.Energy I.Energy vdW Coul NumRotors RMSD Score

ligand_67d2edfaf0_1_run_16.log 1 -19.625 -35.483 7.633 -43.116 7 0.000 -5.813

ligand_67d2edfaf0_1_run_8.log 1 -19.117 -36.858 5.372 -42.230 7 2.445 -5.804

ligand_67d2edfaf0_1_run_4.log 4 -16.689 -32.913 4.288 -37.201 7 2.159 -5.863

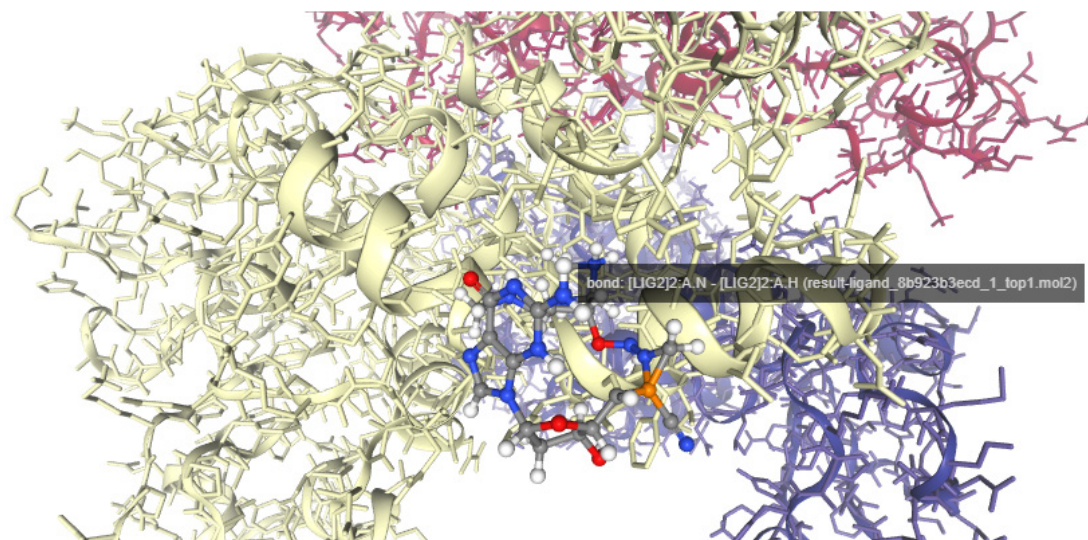


Figure 4b. CoMFA contour map of steric regions (blue, favored; yellow; disfavored) around Roccustyrna; Blue regions are favored by positively charged groups and red regions favored by negatively charged groups inside the SARS-COV-2 protein targets (pdb:6W9C).

File Model T.Energy I.Energy vdW Coul NumRotors RMSD Score

ligand_8b923b3ecd_1_run_2.log 1 -36.678 -55.648 -7.519 -48.129 7 0.000 -6.762

ligand_8b923b3ecd_1_run_16.log 1 -36.224 -53.111 -5.988 -47.123 7 2.941 -6.543

ligand_8b923b3ecd_1_run_4.log 1 -32.903 -52.904 -14.237 -38.667 7 3.940 -7.030

Roccustyrna binding site(s) in 2CME (hypothetical protein 5).

SMALLMOLECULE

D10 (decane)

D10-B-1099

Interacting chains: A, B

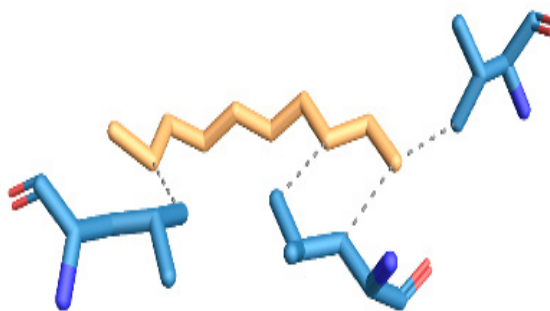


Figure 5a. Roccustyrna binding site(s) in 2CME (hypothetical protein 5).

- Protein
- Ligand
- Water
- Charge Center
- Aromatic Ring Center
- Metal Ion
- Hydrophobic Interaction
- Hydrogen Bond
- Water Bridge
- π -Stacking (parallel)
- π -Stacking (perpendicular)
- π -Cation Interaction
- Halogen Bond
- Salt Bridge
- Metal Complexation

Index	Residue	AA	Distance	Ligand Atom	Protein Atom
1	53A	LEU	3.76	4787	254
2	53B	LEU	3.87	4793	869
3	53B	LEU	3.83	4795	866
4	77B	VAL	3.62	4795	1054

D10-C-1099

Interacting chains: C, D

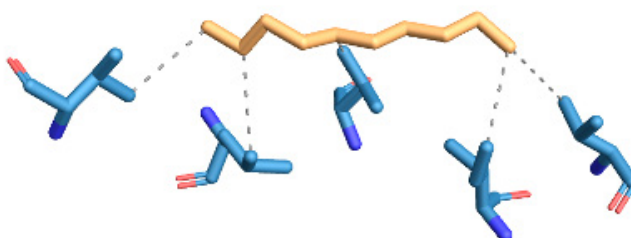


Figure 5a. Roccustyrna binding site(s) in 2CME (hypothetical protein 5).

- Protein
- Ligand
- Water
- Charge Center
- Aromatic Ring Center
- Metal Ion
- Hydrophobic Interaction
- Hydrogen Bond
- Water Bridge
- π -Stacking (parallel)
- π -Stacking (perpendicular)
- π -Cation Interaction
- Halogen Bond
- Salt Bridge
- Metal Complexation

Hydrophobic Interactions

Index	Residue	AA	Distance	Ligand Atom	Protein Atom
1	16C	VAL	4.00	4796	1271
2	45C	ILE	3.83	4796	1400
3	55D	LEU	3.89	4804	2067
4	77D	VAL	3.74	4805	2238
5	95C	VAL	3.96	4801	1787

D10-F-1099

Interacting chains: E, F

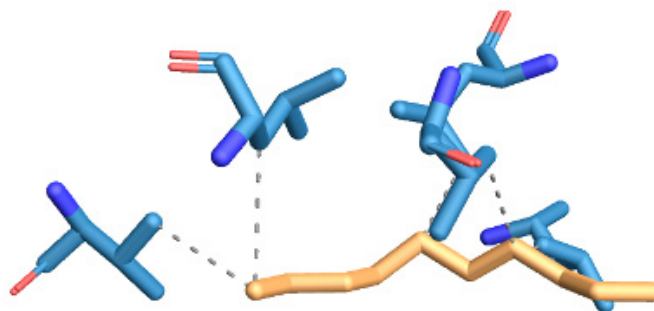


Figure 5c. Roccustyrna binding site(s) in 2CME (hypothetical protein 5) D10-F-1099.

- Protein
- Ligand
- Water
- Charge Center
- Aromatic Ring Center
- Metal Ion
- Hydrophobic Interaction
- Hydrogen Bond
- Water Bridge
- π -Stacking (parallel)
- π -Stacking (perpendicular)
- π -Cation Interaction
- Halogen Bond
- Salt Bridge
- Metal Complexation

Hydrophobic Interactions

Index	Residue	AA	Distance	Ligand Atom	Protein Atom
1	22E	LEU	3.94	4811	2510
2	22F	LEU	3.98	4810	3102
3	55F	LEU	3.85	4815	3255
4	77F	VAL	3.70	4815	3429
5	95E	VAL	3.69	4809	2979

D10-H-1099

Interacting chains: H

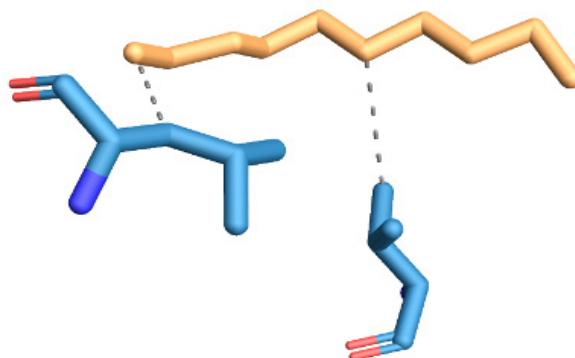
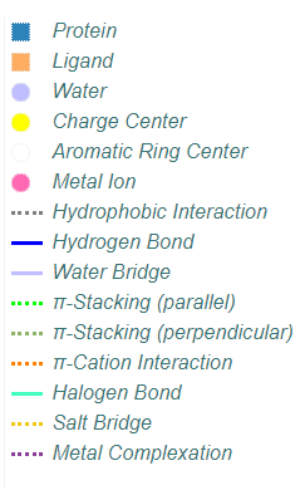


Figure 5d. Roccustyrna binding site(s) in 2CME (hypothetical protein 5) D10-H-1099.



Hydrophobic Interactions

Index	Residue	AA	Distance	Ligand Atom	Protein Atom
1	53H	LEU	3.42	4825	4432
2	95H	VAL	3.89	4820	4762

Prediction of noncovalent interactions for PDB structure 2CME

=====

Created on 2020/11/04 using PLIP v1.4.4

If you are using PLIP in your work, please cite:

Salentin,S. et al. PLIP: fully automated protein-ligand interaction profiler.

Nucl. Acids Res. (1 July 2015) 43 (W1): W443-W447. doi: 10.1093/nar/gkv315

D10:B:1099 (D10) - SMALLMOLECULE

Interacting chain(s): A,B

****Hydrophobic Interactions****

RESNR	RESTYPE	RESCHAIN	RESNR_LIG	RESTYPE_LIG	RESCHAIN_LIG	DIST	LIGCARBONIDX	PROTCARBONIDX	LIGCOO	PROTCOO
53	LEU	A	1099	D10	B	3.76	4787	254	48.955, 23.619, 16.401	47.080, 24.675, 13.313
53	LEU	B	1099	D10	B	3.87	4793	869	52.046, 20.761, 11.577	49.032, 23.137, 11.111
53	LEU	B	1099	D10	B	3.83	4795	866	52.630, 20.477, 9.083	50.000, 23.248, 8.880
77	VAL	B	1099	D10	B	3.62	4795	1054	52.630, 20.477, 9.083	55.494, 18.332, 8.511

D10:C:1099 (D10) - SMALLMOLECULE

Interacting chain(s): C,D

****Hydrophobic Interactions****

RESNR	RESTYPE	RESCHAIN	RESNR_LIG	RESTYPE_LIG	RESCHAIN_LIG	DIST	LIGCARBONIDX	PROTCARBONIDX	LIGCOO	PROTCOO
16	VAL	C	1099	D10	C	4.00	4796	1271	58.394, 53.885, 36.361	61.888, 52.432, 35.074
45	ILE	C	1099	D10	C	3.83	4796	1400	58.394, 53.885, 36.361	60.025, 53.415, 39.796
55	LEU	D	1099	D10	C	3.89	4804	2067	52.052, 48.749, 41.009	55.000, 47.466, 43.193

```

| 77 | VAL | D | 1099 | D10 | C | 3.74 | 4805 | 2238 | 50.737, 47.943, 40.910 | 50.393, 46.300, 44.252 |
+-----+-----+-----+-----+-----+-----+-----+-----+-----+-----+
| 95 | VAL | C | 1099 | D10 | C | 3.96 | 4801 | 1787 | 53.889, 50.872, 39.245 | 55.249, 47.712, 37.280 |
+-----+-----+-----+-----+-----+-----+-----+-----+-----+-----+
D10:F:1099 (D10) - SMALLMOLECULE
-----
Interacting chain(s): E,F
**Hydrophobic Interactions**
+-----+-----+-----+-----+-----+-----+-----+-----+-----+-----+
| RESNR | RESTYPE | RESCHAIN | RESNR_LIG | RESTYPE_LIG | RESCHAIN_LIG | DIST | LIGCARBONIDX | PROTCARBONIDX | LIGCOO | PROTCOO |
+=====+=====+=====+=====+=====+=====+=====+=====+=====+=====+
| 22 | LEU | E | 1099 | D10 | F | 3.94 | 4811 | 2510 | 12.819, 16.563, -3.896 | 14.935, 18.867, -6.285 |
+-----+-----+-----+-----+-----+-----+-----+-----+-----+-----+
| 22 | LEU | F | 1099 | D10 | F | 3.98 | 4810 | 3102 | 13.936, 16.709, -2.837 | 17.300, 18.380, -4.159 |
+-----+-----+-----+-----+-----+-----+-----+-----+-----+-----+
| 55 | LEU | F | 1099 | D10 | F | 3.85 | 4815 | 3255 | 9.250, 13.122, -4.170 | 7.359, 16.230, -5.431 |
+-----+-----+-----+-----+-----+-----+-----+-----+-----+-----+
| 77 | VAL | F | 1099 | D10 | F | 3.70 | 4815 | 3429 | 9.250, 13.122, -4.170 | 8.331, 12.696, -7.725 |
+-----+-----+-----+-----+-----+-----+-----+-----+-----+-----+
| 95 | VAL | E | 1099 | D10 | F | 3.69 | 4809 | 2979 | 13.670, 17.961, -1.962 | 10.282, 19.400, -1.707 |
+-----+-----+-----+-----+-----+-----+-----+-----+-----+-----+
D10:H:1099 (D10) - SMALLMOLECULE
-----
Interacting chain(s): H
**Hydrophobic Interactions**
+-----+-----+-----+-----+-----+-----+-----+-----+-----+-----+
| RESNR | RESTYPE | RESCHAIN | RESNR_LIG | RESTYPE_LIG | RESCHAIN_LIG | DIST | LIGCARBONIDX | PROTCARBONIDX | LIGCOO | PROTCOO |
+=====+=====+=====+=====+=====+=====+=====+=====+=====+=====+
| 53 | LEU | H | 1099 | D10 | H | 3.42 | 4825 | 4432 | 84.803, 13.060, -3.541 | 83.691, 12.515, -0.350 |
+-----+-----+-----+-----+-----+-----+-----+-----+-----+-----+
| 95 | VAL | H | 1099 | D10 | H | 3.89 | 4820 | 4762 | 89.243, 15.969, -1.884 | 91.826, 13.298, -0.741 |
+-----+-----+-----+-----+-----+-----+-----+-----+-----+-----+

```

Results - ROCCUSTYRNATM_6LU7
 2 binding site(s) in 6LU7.
 SMALLMOLECULE
 02J (5-Methylisoxazole-3-carboxylic acid)
 02J-C-1
 Interacting chains: A

- Protein
- Ligand
- Water
- Charge Center
- Aromatic Ring Center
- Metal Ion
- Hydrophobic Interaction
- Hydrogen Bond
- Water Bridge
- ⋯ π -Stacking (parallel)
- ⋯ π -Stacking (perpendicular)
- ⋯ π -Cation Interaction
- Halogen Bond
- ⋯ Salt Bridge
- ⋯ Metal Complexation

Hydrophobic Interactions

Index	Residue	AA	Distance	Ligand Atom	Protein Atom
	168A	PRO	3.53	2369	1303

PJE (composite ligand)

PJE-C-5

Composite ligand consists of PJE:C:5, 010:C:6.

Interacting chains: A

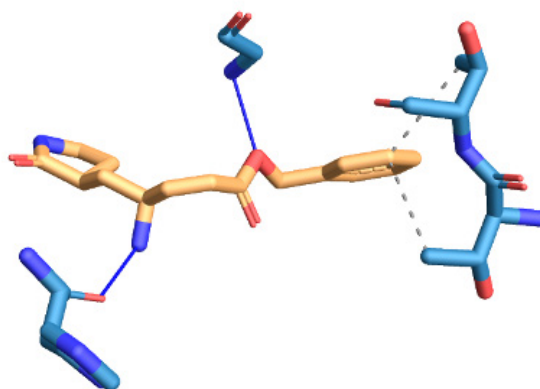


Figure 6b. Rocustyrna binding sites into the 02J (5-Methylisoxazole-3-carboxylic acid) PJE-C-56LU7 protein targets.

- Protein
- Ligand
- Water
- Charge Center
- Aromatic Ring Center
- Metal Ion
- Hydrophobic Interaction
- Hydrogen Bond
- Water Bridge
- π -Stacking (parallel)
- π -Stacking (perpendicular)
- π -Cation Interaction
- Halogen Bond
- Salt Bridge
- Metal Complexation

Hydrophobic Interactions

Index	Residue	AA	Distance	Ligand Atom	Protein Atom
1	25A	THR	3.73	2415	179
2	26A	THR	3.81	2415	186

Hydrogen Bonds

Index	Residue	AA	Distance H-A	Distance D-A	Donor Angle	Protein donor?	Sidechain	Donor Atom	Acceptor Atom
1	143A	GLY	1.93	2.80	145.29	✓	✗	1105 [Nam]	2411 [O3]
2	164A	HIS	2.16	3.07	153.73	✗	✗	2408 [N3]	1266 [O2]

Prediction of noncovalent interactions for PDB structure 6LU7

=====

Created on 2020/11/04 using PLIP v1.4.4

If you are using PLIP in your work, please cite:

Salentin,S. et al. PLIP: fully automated protein-ligand interaction profiler.

Nucl. Acids Res. (1 July 2015) 43 (W1): W443-W447. doi: 10.1093/nar/gkv315

02J:C:1 (02J) - SMALLMOLECULE

Interacting chain(s): A

****Hydrophobic Interactions****

```

+-----+-----+-----+-----+-----+-----+-----+-----+-----+-----+
| RESNR | RESTYPE | RESCHAIN | RESNR_LIG | RESTYPE_LIG | RESCHAIN_LIG | DIST | LIGCARBONIDX | PROTCARBONIDX | LIGCOO | PROTCOO |
+=====+=====+=====+=====+=====+=====+=====+=====+=====+=====+
| 168 | PRO | A | 1 | 02J | C | 3.53 | 2369 | 1303 | -10.425, 3.420, 72.447 | -13.394, 3.190, 70.551 |
+-----+-----+-----+-----+-----+-----+-----+-----+-----+-----+-----+
    
```

PJE:C:5 (PJE-010) - SMALLMOLECULE
 + 010:C:6

Interacting chain(s): A

****Hydrophobic Interactions****

```

+-----+-----+-----+-----+-----+-----+-----+-----+-----+-----+
| RESNR | RESTYPE | RESCHAIN | RESNR_LIG | RESTYPE_LIG | RESCHAIN_LIG | DIST | LIGCARBONIDX | PROTCARBONIDX | LIGCOO | PROTCOO |
+=====+=====+=====+=====+=====+=====+=====+=====+=====+=====+
| 25 | THR | A | 6 | 010 | C | 3.73 | 2415 | 179 | -7.156, 21.406, 66.898 | -8.709, 22.779, 70.002 |
+-----+-----+-----+-----+-----+-----+-----+-----+-----+-----+
    
```

```

+-----+-----+-----+-----+-----+-----+-----+-----+-----+-----+
| 26 | THR | A | 6 | 010 | C | 3.81 | 2415 | 186 | -7.156, 21.406, 66.898 | -6.155, 24.392, 64.757 |
+-----+-----+-----+-----+-----+-----+-----+-----+-----+-----+
    
```

****Hydrogen Bonds****

```

+-----+-----+-----+-----+-----+-----+-----+-----+-----+-----+
| RESNR | RESTYPE | RESCHAIN | RESNR_LIG | RESTYPE_LIG | RESCHAIN_LIG | SIDECHAIN | DIST_H-A | DIST_D-A | DON_ANGLE | PROTISDON |
+=====+=====+=====+=====+=====+=====+=====+=====+=====+=====+
| 143 | GLY | A | 6 | 010 | C | 1.93 | 2.80 | 145.29 | 1105 | Nam | 2411 | O3 | -8.911, 17.849, 65.703 | -8.918, 17.918, 62.905 |
+-----+-----+-----+-----+-----+-----+-----+-----+-----+-----+
    
```

```

+-----+-----+-----+-----+-----+-----+-----+-----+-----+-----+
| 164 | HIS | A | 5 | PJE | C | 2.16 | 3.07 | 153.73 | 2408 | N3 | 1266 | O2 | -12.282, 14.994, 67.123 | -15.161, 15.336, 68.144 |
+-----+-----+-----+-----+-----+-----+-----+-----+-----+-----+
    
```

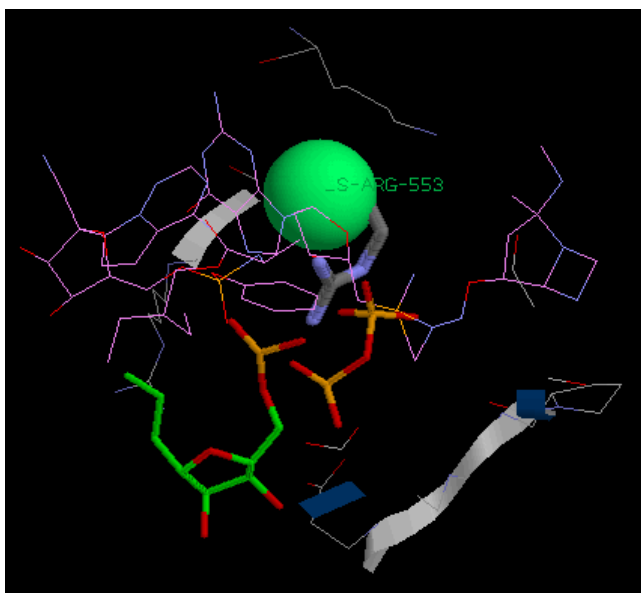


Figure 6c. CoMFA contour map of electrostatic regions around ROCCUFFIRNA CHEMICAL STRUCTURE. Contact residues of the Roccustyrna small molecule when docked onto the SARS-COV-2 protein targets, (pdb:7bv2). (green, favored; yellow; disfavored) around the Roccustyrna chemical structure. Blue regions are favored by positively charged groups and red regions favored by negatively charged groups.

GID	Compound NAME	GWEIGHT	H-S-ARG-553	H-S-ASP-623	H-M-F86-101	H-M-F86-101	V-M-LYS-551	V-S-
LYS-551	V-S-ARG-553	V-S-ARG-555	V-S-ARG-555	V-S-ASP-618	V-M-TYR-619	V-M-PRO-620	V-M-CYS-622	
EWEIGHT			1.0	1.0	1.0	1.0	1.0	1.0
NaN								
GENE0X	cav7bv2_POP-Roccustyrna-0.pdb	cav7bv2_POP-Roccustyrna-0.pdb	1.0	0.0	0.0	0.0	0.0	-4.71516 -10.4842
-4.7999	-2.78895 -6.65538 -5.1339	-6.28532 -0.923983						

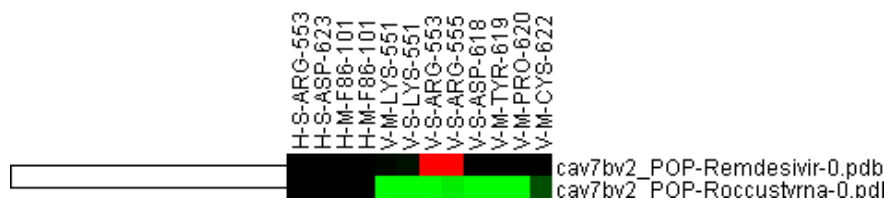


Figure 6d. Comparative Docking Cluster Analysis between the Remdesivir and the Rocustyrna small molecules when docked onto the SARS-COV-2 protein targets, (pdb:7bv2).

	Compound	Energy	V-M LYS 551	V-S LYS 551	V-S ARG 553	V-S ASP 618	V-M TYR 619	V-M PRO 620
1	<input checked="" type="checkbox"/> cav7bv2_POP-Rocustyrna-0.pdb	-66,7	<input checked="" type="checkbox"/> -4,7	<input checked="" type="checkbox"/> -10,5	<input checked="" type="checkbox"/> -4,8	<input checked="" type="checkbox"/> -6,7	<input checked="" type="checkbox"/> -5,1	<input checked="" type="checkbox"/> -6,3
2	<input type="checkbox"/> cav7bv2_POP-Remdesivir-0.pdb	42,1	-0,1	-0,2	25,1	0	0	0

Figure 6e. Comparative Docking Energy Analysis between the Remdesivir and the Rocustyrna small molecules when docked onto the SARS-COV-2 protein targets, (pdb:7bv2).

Table 1a. Docking energy rankings of the physical hit compounds when docked onto the SARS-COV-2 protein targets of the (pdb:6xs6).

#Ligand	Total Energy	VDW	H Bond	Elec	Aver Con Pair
6xs6-1-HexacosanolStructure2D_	-851.935	-851.935	0	0	194.815
6xs6-2-Benzoxazolinone 2737.	-616.351	-616.351	0	0	38.2
6xs6-3-Carboxy-pentanic acid.	912.735	912.735	0	0	289.231
6xs6-5ursane 33.	-708.616	-708.616	0	0	163.333
6xs6-9-cis-Antheraxanthin 2742.	129.936	129.936	0	0	119.535
6xs6-4584RA-XIII.	-486.948	-486.948	0	0	495.714
6xs6-6948crotonate.	-399.075	-399.075	0	0	37.5
6xs6-abyssinica_ CID_3083701.	72.329	72.329	0	0	230.606
6xs6-Acacia_ CID_5320844.	-943.239	-943.239	0	0	200.303
6xs6- acetovanilloneStructure2D_ CID_2214.	-721.685	-721.685	0	0	409.167
6xs6-acteosideStructure2D_ CID_5281800_.	412.805	412.805	0	0	227.955
6xs6- AdenosineStructure2D_ CID_60961.	-722.898	-722.898	0	0	259.474
6xs6-Africanal_ CID_342943.	-249.945	-249.945	0	0	142.222
6xs6-Agarin_ CID_4266.	-561.753	-561.753	0	0	42.875
6xs6-Aloe-emodinStructure2D_ CID_10207.	147.811	147.811	0	0	18.2
6xs6-alpha-L-Rhamnose_ CID_439710.	-54.989	-54.989	0	0	303.636
6xs6-alpha-TocopherolStructure2D_ CID_14985.	238.62	238.62	0	0	210.645
6xs6-alpha-TurmeroneStructure2D_ CID_14632996.	-658.863	-658.863	0	0	24.875
6xs6-Ammonium glycyrrhizate_ CID_62074.	723.806	723.806	0	0	259.831
6xs6-Anemone blue anthocyanin 1_ CID_11979368.	264.373	264.373	0	0	878.022

6xs6-anilineStructure2D_ CID_6115.	-520.154	-520.154	0	0	442.857
6xs6-AnnonaStructure2D_ CID_5459105.	215.215	215.215	0	0	206.818
6xs6-AntitrypsinStructure2D_ CID_165580(1).	-931.264	-931.264	0	0	150.952
6xs6-Arachidonic AcidStructure2D_ CID_444899.	-759.696	-759.696	0	0	211.818
6xs6-Aristolochiac acid C_ CID_165274.	441.074	441.074	0	0	138.333
6xs6-Aristolochic acid_ CID_2236.	-905.713	-905.713	0	0	26.44
6xs6-Asparagusate_ CID_16070001.	-508.316	-508.316	0	0	36.875
6xs6-aspartic acid 101.	-109.242	-109.242	0	0	192.222
6xs6-AstragalinStructure2D_ CID_5282102.	300.38	300.38	0	0	200.313
6xs6-atraric acid 102.	-733.872	-733.872	0	0	322.143
6xs6-AtrazineStructure2D_ CID_2256.	-757.602	-757.602	0	0	36.5
6xs6-avicine103.	145.172	145.172	0	0	21.32
6xs6-azadirachtinStructure2D_ CID_5281303.	171.47	171.47	0	0	130.784
6xs6-Baicalein-7-methyl ether 3673.	-68.083	-68.083	0	0	191.429
6xs6-balanitin 3 106.	663.539	663.539	0	0	13.871
6xs6-balanitin 4 107.	-258.278	-258.278	0	0	19.589
6xs6-balanitin 5 108.	-87.321	-87.321	0	0	994.444
6xs6-balanitin 7 110.	-887.161	-887.161	0	0	93.662
6xs6-baueronol 111.	-707.698	-707.698	0	0	16.129
6xs6-b-Chlorogenin 7651.	-707.493	-707.493	0	0	171.613
6xs6-behenic acid 112.	-746.006	-746.006	0	0	213.333
6xs6-benzo[c]phenanthridine113.	-713.002	-713.002	0	0	321.429
6xs6-Benzyl alcohol 2614.	-47.602	-47.602	0	0	31.875
6xs6-benzyl isothiocyanate (BITC) 114.	907.592	907.592	0	0	24.1
6xs6-benzylic amines 115.	-788.472	-788.472	0	0	8.625
6xs6-Berberine alkaloids 116.	111.594	111.594	0	0	15.44

Table 1b. List of active Rocustyrna fragmented compounds.

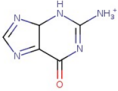
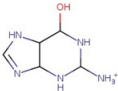
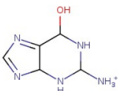
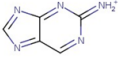
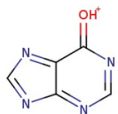
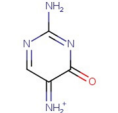
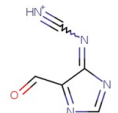
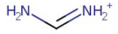
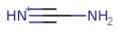
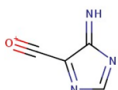
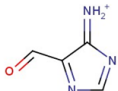
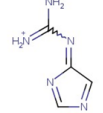
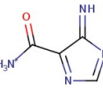
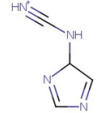
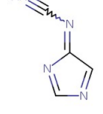
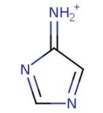
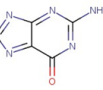
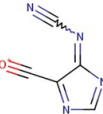
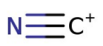
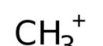
Structure	ID	Mass	SMILES
No Image	0	507.2214365	<chem>CNC1(C)CC(ONN2C[P]2(C#N)CC2OC(n3cnc4c3[nH]c([NH3+])nc4=O)CC2O)C2NCN21</chem>
No Image	1	489.2108718	<chem>CNC1(C)C=C(ONN2C[P]2(C=C2CC=C(N3C=NC4=C(O)N=C([NH3+])N=C43)O2)CN)C2NCN21</chem>
	2	152.0566862	<chem>[NH3+]C1=NC(=O)C2=NC=NC2N1</chem>
	6	158.1036364	<chem>[NH3+]C1NC2N=CNC2C(O)N1</chem>
	7	156.0879864	<chem>[NH3+]C1NC2N=CN=C2C(O)N1</chem>
	8	154.0723363	<chem>[NH3+]C1NC(=O)C2=NC=NC2N1</chem>
	9	134.0461215	<chem>[NH2+]=C1N=CC2=NC=NC2=N1</chem>
			
	10	135.0301371	<chem>[OH+]=C1N=CN=C2N=CN=C21</chem>
	11	125.0457872	<chem>NC1=NC(=O)C(=[NH2+])C=N1</chem>
	12	135.0301371	<chem>[NH+]#CN=C1N=CN=C1C=O</chem>
	13	45.04472458	<chem>NC=[NH2+]</chem>
			
	14	43.02907452	<chem>[NH+]#CN</chem>
			
	15	108.0192381	<chem>N=C1N=CN=C1C#[O+]</chem>
	16	110.0348882	<chem>[NH2+]=C1N=CN=C1C=O</chem>
	17	124.0617716	<chem>NC(=[NH2+])N=C1C=NC=N1</chem>
			
	18	125.0457872	<chem>N=C1N=CN=C1C([NH3+])=O</chem>
			
	19	109.0508726	<chem>[NH+]#CNC1C=NC=N1</chem>
	20	107.0352225	<chem>[NH+]#CN=C1C=NC=N1</chem>
	21	82.03997355	<chem>[NH2+]=C1C=NC=N1</chem>
			
	22	150.0410362	<chem>[NH3+]C1=NC(=O)C2=NC=NC2=N1</chem>
	23	133.0144871	<chem>N#CN=C1N=CN=C1C#[O+]</chem>
	35	26.00252542	<chem>[C+]#N</chem>
			
	99	15.02292652	<chem>[CH3+]</chem>
			

Table 1b. List of active Rocustyrna fragmented compounds.

Ph	Don	Acc
0,0	8,73	11,27
0,50	8,44	11,56
1,00	8,12	11,88
1,50	7,80	12,20
2,00	7,48	12,52
2,50	7,21	12,79
3,00	7,08	12,92
3,50	7,03	12,97
4,00	7,01	12,99
4,50	7,00	13,00
5,00	7,00	13,00
5,50	6,99	13,01
6,00	6,98	13,02
6,50	6,95	13,05
7,00	6,86	13,14

7,50	6,65	13,35
8,00	6,37	13,64
8,50	6,14	13,88
9,00	5,99	14,07
9,50	5,84	14,34
10,00	5,60	14,81
10,50	5,31	15,37
11,00	5,13	15,75
11,50	5,04	15,92
12,00	5,00	15,98
12,50	4,97	16,02

Table 2a. List of smiles of the Roccustyrna active fragments.

energy0
15.02292652 0.9382305843 99 (0.93823)
26.00252542 2.261472925 35 (2.2615)
30.03382555 0.535992489 129 (0.53599)
32.04947561 0.4083831708 128 (0.40838)
109.0760247 0.6306776069 105 (0.63068)
134.0461215 1.054959553 9 (1.055)
134.0712737 0.6753435418 59 (0.67534)
135.0301371 2.00414747 10 12 (1.8344 0.16975)
136.0869237 0.8276811831 33 (0.82768)
138.1025738 5.854997521 4 (5.855)
140.1182239 11.87293119 3 (11.873)
142.1338739 1.434949881 32 (1.4349)
150.0410362 0.7478931696 22 (0.74789)
152.0566862 50.57559424 2 (50.576)
158.1287886 0.5441383792 84 (0.54414)
250.0934657 1.102478867 68 (1.1025)
255.1243482 0.4222794277 39 (0.42228)
256.1195972 0.9300528895 55 34 (0.82641 0.10364)
257.1399983 0.4627232947 148 (0.46272)
258.1352473 0.7827475764 48 (0.78275)
266.1039472 0.4286298007 43 (0.42863)
270.1352473 0.5767642398 40 (0.57676)
272.1508973 1.403710436 30 (1.4037)
335.0890254 0.6614061977 77 (0.66141)
350.0999244 0.5843430157 89 (0.58434)
356.1720267 0.4195737218 25 (0.41957)
472.1843227 0.8241622495 5 (0.82416)
476.1792373 0.8957022747 121 (0.8957)
489.2108718 1.289594322 1 26 (1.1883 0.10129)
490.1948874 3.389865269 147 28 166 173 (2.7809 0.55441 0.043182 0.011359)
507.2214365 5.458573512 0 (5.4586)
Energy 1
26.00252542 1.003424285 35 (1.0034)
108.0192381 0.4484564381 15 (0.44846)
109.0508726 1.550778576 19 (1.5508)
109.0760247 1.307266463 105 (1.3073)
111.0916748 0.514768555 97 115 (0.45789 0.056876)
124.0617716 0.8909860357 17 (0.89099)
134.0461215 1.945717906 9 (1.9457)
135.0301371 4.830634071 10 12 (3.3243 1.5064)
138.1025738 2.758491951 4 (2.7585)
140.1182239 5.537145101 3 (5.5371)
142.1338739 1.502767544 32 (1.5028)
152.0566862 61.84168617 2 (61.842)

171.1240375 0.9257645934 56 (0.92576)
225.0773981 0.6516260185 60 (0.65163)
227.0930481 0.4793912741 52 (0.47939)
229.1086982 0.6269263545 53 (0.62693)
231.1243482 1.055636235 54 (1.0556)
239.0930481 1.005808076 61 (1.0058)
241.1086982 0.8475927077 36 (0.84759)
243.1243482 0.6580287877 37 (0.65803)
245.1399983 1.083243159 38 (1.0832)
253.1086982 0.8138872082 41 (0.81389)
254.1039472 0.7868172629 62 (0.78682)
256.1195972 1.129798814 55 34 (1.0665 0.063267)
258.1352473 1.075725275 48 (1.0757)
268.1195972 0.4895269014 42 (0.48953)
270.1352473 0.4898493769 40 (0.48985)
449.1683383 0.4614633584 144 187 (0.4575 0.0039625)
462.1999728 0.6710353339 135 (0.67104)
480.2105375 1.879432017 134 (1.8794)
490.1948874 0.736324146 147 28 173 166 (0.6098 0.1038 0.016593 0.0061259)
Energy 2
15.02292652 0.995023181 99 (0.99502)
26.00252542 1.024091421 35 (1.0241)
45.04472458 0.9518049313 13 (0.9518)
79.02907452 0.7948376336 118 (0.79484)
80.04947561 3.661453795 119 (3.6615)
81.04472458 1.362092912 109 (1.3621)
82.03997355 1.630942429 21 (1.6309)
82.06512568 0.9001924745 113 (0.90019)
83.06037464 1.196365366 101 (1.1964)
84.08077574 2.268763628 103 (2.2688)
85.07602471 2.328821417 102 (2.3288)
86.0964258 1.087814221 104 (1.0878)
107.0352225 3.067121836 20 (3.0671)
107.0603746 1.010133785 116 (1.0101)
108.0192381 2.161146957 15 (2.1611)
109.0508726 4.111770418 19 (4.1118)
109.0760247 4.299628128 105 (4.2996)
110.0348882 4.444814629 16 (4.4448)
111.0916748 1.715509525 97 115 (1.662 0.053524)
124.0869237 0.6660839118 106 (0.66608)
125.0457872 1.490098898 11 18 (0.97721 0.51289)
126.1025738 1.95890532 100 (1.9589)
134.0461215 5.996375544 9 (5.9964)
135.0301371 15.39694322 12 10 (10.757 4.6396)
136.0869237 1.902630549 33 (1.9026)
138.1025738 5.083500848 4 (5.0835)
140.1182239 5.729483613 3 (5.7295)
142.1338739 1.748821474 32 (1.7488)
150.0410362 1.320314853 22 (1.3203)
152.0566862 18.90373723 2 (18.904)
356.1720267 0.7907758483 25 (0.79078)
0 507.2214365 CNC1(C)CC(ONN2C[P]2(C#N)CC2OC(n3cnc4c3[nH]c([NH3+])nc4=O)CC2O)C2NCN21
1 489.2108718 CNC1(C)C=C(ONN2C[P]2(C=C2CC=C(N3C=NC4=C(O)N=C([NH3+])N=C43)O2)CN)C2NCN21
2 152.0566862 [NH3+][C1=NC(=O)C2=NC=NC2N1
3 140.1182239 C[NH2+][C1(C)C=CC2NCN21
4 138.1025738 C[NH2+][C1(C)C=CC2=NCN21
5 472.1843227 CNC1(C)C=C(ONN2C[P]2(C)C=C2CC=C(N3C=NC4=C(O)N=C([NH3+])N=C43)O2)C2=NCN21

6 158.1036364 [NH3+]C1NC2N=CNC2C(O)N1	63 237.0773981 C#[N+]C1(C)C=C(ONN2C[P]2=C)C2=NCN21
7 156.0879864 [NH3+]C1NC2N=CN=C2C(O)N1	64 252.0882971 C=NC1(C)C=C(O[NH2+]N2C[P]2=C=N)C2=NCN21
8 154.0723363 [NH3+]C1NC(=O)C2=NC=NC2N1	65 250.072647 C#[N+]C1(C)C=C(ONN2C[P]2=C=N)C2=NCN21
9 134.0461215 [NH2+]=C1N=CC2=NC=NC2=N1	66 246.0621655 C=C1OC(N2C=NC3=C(O)N=C([NH3+])N=C32)=CC1=O
10 135.0301371 [OH+]=C1N=CN=C2N=CN=C21	67 248.0778156 CC1OC(N2C=NC3=C(O)N=C([NH3+])N=C32)=CC1=O
11 125.0457872 NC1=NC(=O)C(=[NH2+])C=N1	68 250.0934657 CC1OC(N2C=NC3=C(O)N=C([NH3+])NC32)=CC1=O
12 135.0301371 [NH+]#CN=C1N=CN=C1C=O	69 232.082901 C=C1CC=C(N2C=NC3=C(O)N=C([NH3+])N=C32)O1
13 45.04472458 NC=[NH2+]	70 252.1091157 CC1OC(N2C=NC3=C(O)NC([NH3+])NC32)=CC1=O
14 43.02907452 [NH+]#CN	71 254.1247658 CC1OC(N2C=NC3C2NC([NH3+])NC3O)=CC1=O
15 108.0192381 N=C1N=CN=C1C#[O+]	72 256.1404159 CC1OC(N2CNC3C2NC([NH3+])NC3O)=CC1=O
16 110.0348882 [NH2+]=C1N=CN=C1C=O	73 258.1560659 CC1OC(N2CNC3C2NC([NH3+])NC3O)=CC1O
17 124.0617716 NC(=[NH2+])N=C1C=NC=N1	74 173.1396876 CNC1(C)CC(O[NH3+])C2NCN21
18 125.0457872 N=C1N=CN=C1C([NH3+])=O	75 140.0818384 CC1C=C(O[NH3+])C2=NCN21
19 109.0508726 [NH+]#CNC1C=NC=N1	76 167.0927374 C=NC1(C)C=C(O[NH3+])C2=NCN21
20 107.0352225 [NH+]#CN=C1C=NC=N1	77 335.0890254 NC[P]1(C=C2OC(N3C=NC4=C(O)N=C([NH3+])N=C43)=CC2=O)CN1
21 82.03997355 [NH2+]=C1C=NC=N1	78 100.0184862 C[P]1(C#[NH+])C=N1
22 150.0410362 [NH3+]C1=NC(=O)C2=NC=NC2=N1	79 318.0624763 C[P]1(C=C2OC(N3C=NC4=C(O)N=C([NH3+])N=C43)=CC2=O)C=N1
23 133.0144871 N#CN=C1N=CN=C1C#[O+]	80 337.1046754 NC[P]1(CC2OC(N3C=NC4=C(O)N=C([NH3+])N=C43)=CC2=O)CN1
24 354.1563766 CNC1(C)C=C(O[NH2+]N2C[P]2(C=C2OC=CC2=O)CN)C2NCN21	81 339.1203255 NC[P]1(CC2OC(N3C=NC4=C(O)N=C([NH3+])NC43)=CC2=O)CN1
25 356.1720267 CNC1(C)CC(O[NH2+]N2C[P]2(C=C2OC=CC2=O)CN)C2NCN21	82 341.1359756 NC[P]1(CC2OC(N3C=NC4=C(O)NC([NH3+])NC43)=CC2=O)CN1
26 489.2108718 CNC1(C)CC(ONN2C[P]2(C=C2OC(N3C=NC4=CN=C([NH3+])N=C43)=CC2=O)CN)C2NCN21	83 343.1516256 NC[P]1(CC2OC(N3C=NC4C3NC([NH3+])NC4O)=CC2=O)CN1
27 136.0617716 [NH2+]=C1N=CC2=NC=NC2N1	84 158.1287886 C[NH2+]C1(C)CC(O)C2NCN21
28 490.1948874 CNC1(C)CC(O[NH2+]N2C[P]2(C=C2OC(N3C=NC4=C(O)N=CN=C43)=CC2=O)CN)C2NCN21	85 142.0974884 CC1([NH3+])CC(=O)C2NCN21
29 274.1665474 CNC1(C)C=C(O[NH2+]N2C[P]2(C)CN)C2NCN21	86 125.0709393 CC1=CC(=[OH+])C2NCN12
30 272.1508973 CNC1(C)C=C(O[NH2+]N2C[P]2(C)CN)C2=NCN21	87 152.0818384 C=[NH+]C1(C)CC(=O)C2=NCN21
31 102.0341363 C[P]1(C=[NH2+])C=N1	88 150.0661883 C#[N+]C1(C)CC(=O)C2=NCN21
32 142.1338739 C[NH2+]C1(C)CCC2NCN21	89 350.0999244 NC[P]1(C=C2OC(N3C=NC4=C(O)N=C([NH3+])N=C43)=CC2=O)CN1N
33 136.0869237 C=[NH+]C1(C)C=CC2=NCN21	90 332.0893597 N#C[P]1(C=C2CC=C(N3C=NC4=C(O)N=C([NH3+])N=C43)O2)CN1N
34 256.1195972 CC1(N)C=C(O[NH2+]N2C[P]2(C)C=N)C2=NCN21	91 115.0293852 [CH2+] [P]1(C#N)CN1N
35 26.00252542 [C+]#N	92 333.0733753 C[P]1([C+]=C2OC(N3C=NC4=C(O)N=C(N)N=C43)=CC2=O)CN1N
36 241.1086982 C=[P]1CN1[NH2+]OC1=CC(C)(NC)N2CN=C12	93 352.1155745 NC[P]1(CC2OC(N3C=NC4=C(O)N=C([NH3+])N=C43)=CC2=O)CN1N
37 243.1243482 C=[P]1CN1[NH2+]OC1=CC(C)(NC)N2CNC12	94 354.1312245 NC[P]1(CC2OC(N3C=NC4=C(O)N=C([NH3+])NC43)=CC2=O)CN1N
38 245.1399983 C=[P]1CN1[NH2+]OC1CC(C)(NC)N2CNC12	95 356.1468746 NC[P]1(CC2OC(N3C=NC4=C(O)NC([NH3+])NC43)=CC2=O)CN1N
39 255.1243482 C=NC1(C)C=C(O[NH2+]N2C[P]2(C)C)C2=NCN21	96 358.1625246 NC[P]1(CC2OC(N3C=NC4C3NC([NH3+])NC4O)=CC2=O)CN1N
40 270.1352473 C=NC1(C)C=C(O[NH2+]N2C[P]2(C)CN)C2=NCN21	97 111.0916748 [CH4+]C1C=CC2NCN21
41 253.1086982 C#[N+]C1(C)C=C(ONN2C[P]2(C)C)C2=NCN21	98 113.1073248 [CH4+]C1CCC2NCN21
42 268.1195972 C=NC1(C)C=C(O[NH2+]N2C[P]2(C)C=N)C2=NCN21	99 15.02292652 [CH3+]
43 266.1039472 C=NC1(C)C=C(O[NH2+]N2C[P]2(C)C#N)C2=NCN21	100 126.1025738 CC1([NH3+])C=CC2NCN21
44 264.0882971 C#[N+]C1(C)C=C(ONN2C[P]2(C)C#N)C2=NCN21	101 83.06037464 C#[CH+]C1CN1
45 234.0621655 [NH3+]C1=NC(O)=C2N=CN(C3=CC(=O)CO3)C2=N1	102 85.07602471 C=[CH2+]C1CN1
46 236.0778156 [NH3+]C1=NC(O)=C2N=CN(C3=CC(=O)CO3)C2N1	103 84.08077574 C#CC(C)[NH2+]C
47 262.1665474 CNC1(C)CC(O[NH2+]N2C[PH]2CN)C2NCN21	104 86.0964258 C=CC(C)[NH2+]C
48 258.1352473 CNC1(C)C=C(O[NH2+]N2C[PH]2CN)C2=NCN21	105 109.0760247 [CH4+]C1C=CC2=NCN21
49 86.00283615 [NH+]#C[P]1=NC1	106 124.0869237 C[NH2+]C1C=CC2=NCN21
50 88.01848621 [NH2+]=C[P]1=NC1	107 60.08077574 CC[NH2+]C
51 242.1039472 CC1(N)C=C(O[NH2+]N2C[P]2=CN)C2=NCN21	108 56.04947561 C=C=[NH+]C
52 227.0930481 C=NC1(C)C=C(O[NH2+]N2C[PH]2)C2=NCN21	109 81.04472458 C#[CH+]C1=NCN1
53 229.1086982 CNC1(C)C=C(O[NH2+]N2C[PH]2)C2=NCN21	110 87.09167477 C[CH3+]C1CN1
54 231.1243482 CNC1(C)C=C(O[NH2+]N2C[PH]2)C2NCN21	111 112.0869237 C[NH+]C(N)C=NC1
55 256.1195972 C=NC1(C)C=C(O[NH2+]N2C[PH]2CN)C2=NCN21	112 59.06037464 C1NC[NH2+]1
56 171.1240375 CNC1(C)C=C(O[NH3+])C2NCN21	
57 156.1131385 C[NH2+]C1(C)CC(=O)C2NCN21	
58 101.0137352 N#C[P]1=CN1[NH3+]	
59 134.0712737 C#[N+]C1(C)C=CC2=NCN21	
60 225.0773981 C=C1C=C(O[NH2+]N2C[P]2=CN)C2=NCN21	
61 239.0930481 C=NC1(C)C=C(O[NH2+]N2C[P]2=C)C2=NCN21	
62 254.1039472 C=NC1(C)C=C(O[NH2+]N2C[P]2=CN)C2=NCN21	

113 82.06512568 C#CC(C)=[NH+J	155 180.0516009 [NH3+J]C1=NC(O)=C2N=CN(C=O)C2=N1
114 113.1073248 C[NH2+J]C1(C)C=CCN1	156 178.0359508 NC1=NC(O)=C2N=CN(C#O)C2=N1
115 111.0916748 C[NH2+J]C1(C)C=CC=N1	157 326.161462 C=C(O)C#C[P]1(CN)CN1[NH2+J]OC1=CC(C)(NC)N2CNC12
116 107.0603746 [CH3+]=C1C=CC2=NCN21	158 204.0516009 [NH3+J]C1=NC(O)=C2N=CN(C#CC=O)C2=N1
117 122.0712737 [CH2+J]C1(N)C=CC2=NCN21	159 206.0672509 [NH3+J]C1=NC(O)=C2N=CN(C#CC=O)C2N1
118 79.02907452 C#[CH+J]C1=NC=N1	160 208.082901 [NH3+J]C1NC(O)=C2N=CN(C#CC=O)C2N1
119 80.04947561 C#CC(C)=[N+J]=C	161 210.098551 [NH3+J]C1NC2C(N=CN2C#CC=O)C(O)N1
120 368.1104891 NC[P]1(CC2OC(N3C=NC4=C(O)N=C([NH3+])N=C43)=CC2=O)CN1NO	162 330.1563766 CNC1(C)C=C(O)[NH2+J]N2C[P]2(CN)CC(=O)C=O)C2N2CN21
121 476.1792373 CC1CC(ONN2C[P]2(C=C2OC(N3C=NC4=C(O)N=C([NH3+])N=C43)=CC2=O)CN)C2N2CN21	163 174.0410362 [C+J]#CN1C=NC2=C(O)N=C(N)N=C21
122 458.1686726 CC1C=C(ONN2C[P]2(C=C2CC=C(N3C=NC4=C(O)N=C([NH3+])N=C43)O2)CN)C2=NCN21	164 176.0566862 C#CN1C=NC2=C(O)N=C([NH3+])N=C21
123 241.1086982 C=C1C=C(O)[NH2+J]N2C[P]2(C)CN)C2=NCN21	165 180.0879864 C#CN1C=NC2=C(O)NC([NH3+])NC21
124 459.1526882 CC1C=C(ONN2C[P]2(C)C=C2OC(N3C=NC4=C(O)N=C([NH3+])N=C43)=CC2=O)C2N2CN21	166 490.1948874 CNC1(C)CC(ONN2C[P]2(CN)CC2OC(N3C=NC(=C=O)C3=NC#[NH+])=CC2=O)C2N2CN21
125 480.2105375 CC1CC(ONN2C[P]2(CN)CC2OC(N3C=NC4=C(O)N=C([NH3+])NC43)=CC2=O)C2N2CN21	167 137.0457872 [NH+J]#CNC1N=CN=C1C=O
126 491.1901364 CC1(N)CC(ONN2C[P]2(C=C2OC(N3C=NC4=C(O)N=C([NH3+])N=C43)=CC2=O)CN)C2N2CN21	168 463.1839884 CNC1(C)CC(ONN2C[P]2(C=C2OC(N3C=NC(=C=O)C3=[NH2+])=CC2=O)CN)C2N2CN21
127 491.1901364 CNC1CC(ONN2C[P]2(C=C2OC(N3C=NC4=C(O)N=C([NH3+])N=C43)=CC2=O)CN)C2N2CN21	169 465.1996384 CNC1(C)CC(ONN2C[P]2(CN)CC2OC(N3C=NC(=C=O)C3=[NH2+])=CC2=O)C2N2CN21
128 32.04947561 C[NH3+]	170 479.2265219 CNC1(C)CC(ONN2C[P]2(C=C2OC(N3C=NCC3=NC(N)=[NH2+])=CC2=O)CN)C2N2CN21
129 30.03382555 C=[NH2+]	171 464.2156228 CNC1(C)CC(ONN2C[P]2(CN)CC2OC(N3C=NCC3=NC#[NH+])=CC2=O)C2N2CN21
130 476.1792373 CNC1(C)CC(ONN2C[PH]2C=C2OC(N3C=NC4=C(O)N=C([NH3+])N=C43)=CC2=O)C2N2CN21	172 462.1999728 CNC1(C)CC(ONN2C[P]2(C=C2OC(N3C=NCC3=NC#[NH+])=CC2=O)CN)C2N2CN21
131 458.1686726 CNC1(C)C=C(ONN2C[P]2(C=C2CC=C(N3C=NC4=C(O)N=C([NH3+])N=C43)O2)C2N2CN21	173 490.1948874 CNC1(C)C=C(ONN2C[P]2(C=C2OC(N3C=NC(=C(O)[NH+]=C=N)C3)=CC2=O)CN)C2N2CN21
132 478.1948874 CNC1(C)CC(ONN2C[PH]2CC2OC(N3C=NC4=C(O)N=C([NH3+])N=C43)=CC2=O)C2N2CN21	174 437.2047238 CNC1(C)CC(ONN2C[P]2(C=C2OC(N3C=NCC3=[NH2+])=C2=O)CN)C2N2CN21
133 460.1843227 CNC1(C)CC(ONN2C[P]2(C=C2CC=C(N3C=NC4=C(O)N=C([NH3+])N=C43)O2)C2N2CN21	175 86.03488817 N=C(N)[NH+]=C=O
134 480.2105375 CNC1(C)CC(ONN2C[PH]2CC2OC(N3C=NC4=C(O)N=C([NH3+])NC43)=CC2=O)C2N2CN21	176 322.0937764 C[PH]1(C=C1OC(N2C=NC3=C(O)N=C([NH3+])N=C32)=CC1=O)CN
135 462.1999728 CNC1(C)CC(ONN2C[PH]2C=C2CC=C(N3C=NC4=C(O)N=C([NH3+])N=C43)O2)C2N2CN21	177 320.0781263 C[P]1(C=C1OC(N2C=NC3=C(O)N=C([NH3+])N=C32)=CC1=O)CN
136 247.1556484 CNC1(C)CC(O)[NH2+J]N2C[PH]2C)C2N2CN21	178 184.1192865 CNC1(C)C=C(ON=[NH2+J])C2N2CN21
137 233.1399983 CNC1(C)CC(O)[NH2+J]N2C[PH]2)C2N2CN21	179 188.1505866 CNC1(C)CC(ON[NH3+J])C2N2CN21
138 308.0781263 [NH3+J]C1=NC(O)=C2N=CN(C3=CC(=O)C(C[PH]4CN4)O3)C2=N1	180 200.1505866 C=[NH+J]NOC1CC(C)(NC)N2CNC12
139 310.0937764 [NH3+J]C1=NC(O)=C2N=CN(C3=CC(=O)C(C[PH]4CN4)O3)C2N1	181 198.1349366 C=[NH+J]NOC1=CC(C)(NC)N2CNC12
140 312.1094265 [NH3+J]C1NC(O)=C2N=CN(C3=CC(=O)C(C[PH]4CN4)O3)C2N1	182 306.0624763 NC[PH]=C=C1OC(N2C=NC3=C(O)N=C([NH3+])N=C32)=CC1=O
141 323.0890254 NN1C[PH]1CC1OC(N2C=NC3=C(O)N=C([NH3+])N=C32)=CC1=O	183 308.0781263 NC[PH2]C=C1OC(N2C=NC3=C(O)N=C([NH3+])N=C32)=CC1=O
142 325.1046754 NN1C[PH]1CC1OC(N2C=NC3=C(O)N=C([NH3+])NC32)=CC1=O	184 310.0937764 NC[PH2]CC1OC(N2C=NC3=C(O)N=C([NH3+])N=C32)=CC1=O
143 327.1203255 NN1C[PH]1CC1OC(N2C=NC3=C(O)NC([NH3+])NC32)=CC1=O	185 438.1635873 NC[P]1(CC2OC(N3C=NC4=C(O)N=C([NH3+])N=C43)=CC2=O)CN1NOCC1NCN1
144 449.1683383 CC1CC(ONN2C[PH]2CC2OC(N3C=NC4=C(O)N=C([NH3+])N=C43)=CC2=O)C2N2CN21	186 451.1839884 CNC(C)CCONN1C[P]1(C=C1OC(N2C=NC3=C(O)N=C([NH3+])N=C32)=CC1=O)CN
145 186.1349366 CNC1(C)CC(ON=[NH2+J])C2N2CN21	187 449.1683383 CNC(C)C=CONN1C[P]1(C=C1OC(N2C=NC3=C(O)N=C([NH3+])N=C32)=CC1=O)CN
146 281.0672273 [NH3+J]C1=NC(O)=C2N=CN(C3=CC(=O)C(C[PH3])O3)C2=N1	188 456.2105375 CC(ONN1C[P]1(CN)CC1OC(N2C=NC3=C(O)NC([NH3+])NC32)=CC1=O)C1NCN1
147 490.1948874 CNC1(C)CC(ONN2C[P]2(C)C=C2OC(N3C=NC4=C(O)N=C([NH3+])N=C43)=CC2=O)C2N2CN21	189 454.1948874 CC(ONN1C[P]1(CN)CC1OC(N2C=NC3=C(O)N=C([NH3+])NC32)=CC1=O)C1NCN1
148 257.1399983 CNC1(C)C=C(O)[NH2+J]N2C[P]2(C)C)C2=NCN21	190 452.1792373 CC(ONN1C[P]1(CN)CC1OC(N2C=NC3=C(O)N=C([NH3+])N=C32)=CC1=O)C1NCN1
149 461.1683383 CC1CC(ONN2C[P]2(C)C=C2OC(N3C=NC4=C(O)N=C([NH3+])N=C43)=CC2=O)C2N2CN21	191 450.1635873 CC(ONN1C[P]1(C=C1OC(N2C=NC3=C(O)N=C([NH3+])N=C32)=CC1=O)CN)C1NCN1
150 224.0778156 [NH3+J]C1NC(O)=C2N=CN(C=O)C=C=O)C2N1	192 55.02907452 C1=NC=[NH+J]1
151 280.1195972 C#C[P]1(CN)CN1[NH2+J]OC1=CC(C)(N=C)N2CN=C12	193 448.1479372 C=C(ONN1C[P]1(C=C1OC(N2C=NC3=C(O)N=C([NH3+])N=C32)=CC1=O)CN)C1NCN1
152 186.098551 [NH3+J]C1NC2C(N=CN2C=O)C(O)N1	194 44.04947561 CC=[NH2+J]
153 184.082901 [NH3+J]C1NC(O)=C2N=CN(C=O)C2N1	195 478.1948874 CNC1(C)CC(ONN2C[P]2(C=C2OC(N3C=NC4=C(O)N=C([NH3+])N=C43)=CC2=O)CN)CN1
154 182.0672509 [NH3+J]C1=NC(O)=C2N=CN(C=O)C2N1	

Discussion

In this article, we propose an alternative topological quantum computing optimization framework for the computation of topological invariants of knots, links and tangles through a stochastic discrete optimization procedure that uses ground structure approach, nonlinear finite element analysis, and quantum-inspired evolutionary algorithms in which the concepts of proper time and rest mass enter in the non-relativistic limit. The focus of this work is to develop a fragmentation algorithm that is as independent as possible from the chosen fragmentation scheme to allow for a faster development of new group contribution methods. For this reason, the Roccustyrna multi-targeted pharmacophoric element for each pattern was kept as simple as possible and can be geometrically represented with logical atomic spaces and subatomic subspaces allowing a vectorial negative docking energy representation. The few chemical patterns (that were made more specific to match the results better from the literature database have been underlined in this project as orthogonally applied for the design of a novel multi-chemo-structure the Roccustyrna small molecule against the crystal structure of COVID-19 main protease in complex with an inhibitor N3 in a Lindenbaum-Tarski generated generated QSAR automating modeling lead compound design approach. In this hybrid drug designing approach, we have designed the RoccustyrnaTM nano-structures as a system of intrinsically positioned cables filtered before evaluation and triangular bars kinematically stable and structurally valid symmetric formations of connected components, holes, and voids jointed at their ends by hinged connections to form a rigid chemical scaffold for calculating Betti numbers-the numbers-in persistent homology.

Conclusion

Here, for the first time we have generated three coupled harmonic oscillators as orthogonally applied for the design of a quantum thinking novel multi-chemo-structure against the crystal structure of COVID-19 main protease, the RoccustyrnaTM small molecule by applying the Biogenetoligandorol algorithm, a Gravitational Topological (UFs) based Quantum-Parallel Particle Swarm Inspired framework using only 2D chemical features that are less compute-intensive in which a generalized procedure of Quantization of classical heuristic fields that can be fused together with QSAR automating modeling. The strategies developed and implemented for the two algorithms using Topology Euclidean Geometric and Artificial Intelligence-Driven Predictive Neural Networks in this work, show that it is possible to automate group fragmentation based on computed descriptors for the patterns in the fragmentation scheme to make use of partial chemical derivatives with the additional difficulty that the drug designs we deal with are not orthogonal. Both algorithms applied in this project are capable of fragmenting every molecule of a reference database of structures into their respective UNIFAC groups. Furthermore, the heuristic algorithms which were used in this project are capable of fragmenting and remerging small molecules that could not be fragmented by the algorithm of the reference database. We have illustrated the power of such an approach interpreted as distinct quantum circuit, qubit preparations, and certain 1- and 2-qudit gates in a meaningful application to components, such as qubits. Our Biogenetoligandorol platform also offers utility to researchers simply wishing to interrogate and organize generalized Hadamard and control-Z gates data, as it can be applied to create an inventory of available numerical docking data with particular clinical or genomic features, of the shaded tangle into two-dimensional space such as available datasets or patients with particular mutations, which may be used to draw independently of its drug identification capabilities. More specifically, in this project we implemented Inverse Docking Algorithms with nonlinear electrodynamics indicated to us that the Roccustyrna TM small molecules exert the highest inhibitory activities and negative docking energies as compared to other FDAs against the same SARS-COV-2 viruses protein targets and while it is probably true that the injudicious use of these ideas can cause problems, it is also true that they do and should play a role quantum mechanically in the this drug discovery field.

References

- Hui, David S. "Epidemic and Emerging Coronaviruses (Severe Acute Respiratory Syndrome and Middle East Respiratory Syndrome)." *Clin Chest Med* 38(2017):71-86.
- Zhu, Na, Dingyu Zhang, Wenling Wang, and Xingwang Li, et al. "Novel Coronavirus from Patients with Pneumonia in China, 2019." *N Engl J Med* 382(2020): 727-733.
- Paraskevis, Dimitrios, Evangelia Georgia Kostaki, Gkikas Magiorkinis, and Georgios Panayiotakopoulos, et al. "Full-genome evolutionary analysis of the novel coronavirus (2019-nCoV) rejects the hypothesis of emergence as a result of a recent recombination event." *Infect Genet Evol* 79(2020): 104212.
- Lu, Roujian, Xiang Zhao, Juan Li, and Peihua Niu, et al. "Genomic characterisation and epidemiology of 2019 novel coronavirus: implications for virus origins and receptor binding." *Lancet* 395(2020): 565-574.
- Luk, Hayes KH, Xin Li, Joshua Fung, and Susanna KP Lau, et al. "Molecular epidemiology, evolution and phylogeny of SARS coronavirus." *Infect Genet Evol* 71(2019): 21-30.
- Ziebuhr, John. "Molecular biology of severe acute respiratory syndrome coronavirus." *Curr Opin Microbiol* 7(2004): 412-419.
- Weiss, Susan R, and Julian L Leibowitz "Coronavirus pathogenesis." *Adv Virus Res* 81(2011): 85-164.
- Brian DA, Baric RS. "Coronavirus genome structure and replication." *Curr Top Microbiol Immunol* 287(2005): 1-30.
- Narayanan, Krishna, Cheng Huang, and Shinji Makino. "SARS coronavirus accessory proteins." *Virus Res* 133(2008): 113-221.
- Arndt, Ariel L, Blake J. Larson, and Brenda G. Hogue. "A conserved domain in the coronavirus membrane protein tail is important for virus assembly." *J Virol* 84(2010): 11418-11428.
- Neuman, Benjamin W, Gabriella Kiss, Andreas H. Kunding, and David Bhella, et al. "A structural analysis of M protein in coronavirus assembly and morphology." *J Struct Biol* 174(2011): 11-22.
- Siu, Kam-Leung, Chi-Ping Chan, Kin-Hang Kok, and Patrick Chiu-Yat Woo, et al. Suppression of innate antiviral response by severe acute respiratory syndrome coronavirus M protein is mediated through the first transmembrane domain. *Cell Mol Immunol* 11(2014): 141-149.
- Schoeman, Dewald, and Burtram C. Coronavirus envelope protein: current knowledge. *Viral J* 16(2019): 69.
- Al-Tawfiq, Jaffar A, Ali H Al-Homoud, and Ziad A. Memish. Remdesivir as a possible therapeutic option for the COVID-19. *Travel Med Infect Dis* (2020):101615.
- Agostini, Maria L, Erica L Andres, Amy C Sims, and Rachel L Graham, et al. Coronavirus Susceptibility to the Antiviral Remdesivir (GS-5734) Is Mediated by the Viral Polymerase and the Proofreading Exoribonuclease. *mBio* 9(2018).
- de Wit, Emmie, Friederike Feldmann, Jacqueline Cronin, and Robert Jordan, et al. Prophylactic and therapeutic remdesivir (GS-5734) treatment in the rhesus macaque model of MERS-CoV infection. *Proc Natl Acad Sci* 12(2020): 6771-6776.
- Lim, Jaegyun, Seunghyun Jeon, Hyun-Young Shin, and Moon Jung Kim, et al. Case of the Index Patient Who Caused Tertiary Transmission of Coronavirus Disease 2019 in Korea: the Application of Lopinavir/Ritonavir for the Treatment of COVID-19 Pneumonia Monitored by Quantitative RT-PCR. *J Korean Med Sci* 35(2020): e88.
- Khot WY, Nadkar MY. The 2019 Novel Coronavirus Outbreak-A Global Threat. *J Assoc Physicians India* 68(2020): 67-71.
- Zeng, Yan-Ming, Xiao-Lei Xu, Xiao-Qing He, and Sheng-Quan Tang, et al. Comparative effectiveness and safety of ribavirin plus interferon-alpha, lopinavir/ritonavir plus interferon-alpha and ribavirin plus lopinavir/ritonavir plus interferon-alpha in patients with mild to moderate novel coronavirus pneumonia. *Chin Med J* 9(2020): 1132-1134.
- Wang, Zhenwei, Xiaorong Chen, Yunfei Lu, Feifei Chen, and Wei Zhang. Clinical characteristics and therapeutic procedure for four cases with 2019 novel coronavirus pneumonia receiving combined Chinese and Western medicine treatment. *Biosci Trends* 14(2020): 64-68.

21. Martinez, Miguel Angel. Compounds with therapeutic potential against novel respiratory 2019 coronavirus. *Antimicrob Agents Chemother* (2020).
22. Gordon, Calvin J, Egor P Tchessnokov, Joy Y Feng, and Danielle P Porter. The antiviral compound remdesivir potently inhibits RNA-dependent RNA polymerase from Middle East respiratory syndrome coronavirus. *J Biol Chem* (2020).
23. Sheahan, Timothy P, Amy C Sims, Sarah R Leist, Alexandra Schäfer, et al. Comparative therapeutic efficacy of remdesivir and combination lopinavir, ritonavir, and interferon beta against MERS-CoV. *Nat Commun* 11(2020): 222.
24. Trott, Oleg, and Arthur J Olson. AutoDock Vina: improving the speed and accuracy of docking with a new scoring function, efficient optimization, and multithreading. *J Comput Chem* 31(2010): 455-461.
25. Van Meter, Rodney, Takahiko Satoh, Thaddeus D Ladd, William J Munro, et al. Path selection for quantum repeater networks. *Networking Science* 3(2013): 82-95.
26. Lloyd, Seth, Masoud Mohseni, and Patrick Rebentrost. Quantum principal component analysis. *Nature Physics* 10(2014): 631.
27. Howlader, Prosenjit, and Mohua Banerjee. Object Oriented Protoconcepts and Logics for Double and Pure Double Boolean Algebras. *Rough Sets. International Joint Conference on Rough Sets* (2020): 308-323.
28. Gyongyosi, Laszlo. Quantum Imaging of High-Dimensional Hilbert Spaces with Radon Transform. *International Journal of Circuit Theory and Applications* 45(2017): 1029-1046.
29. Yuan, Zhen-Sheng, Yu-Ao Chen, Bo Zhao, Shuai Chen, et al. Experimental demonstration of a BDCZ quantum repeater node. *Nature* 454(2008): 1098-1101.
30. Di Caro, Gianni, Frederick Ducatelle, and Luca Maria Gambardella. AdHocNet: An Adaptive Nature-Inspired Algorithm for Routing in Mobile Ad-Hoc Networks. *European Transactions on Telecommunications* 16(2005): 443-455.
31. Chou, Chin-Wen, Julien Laurat, Hui Deng, Kyung Soo Choi, et al. Functional quantum nodes for entanglement distribution over scalable quantum networks. *Science* 316(2007): 1316-1320.
32. Kimble, H. Jeff. The quantum Internet. *Nature* 453(2008): 1023-1030.
33. Gyongyosi, Laszlo. The Correlation Conversion Property of Quantum Channels. *Quantum Information Processing* 13(2014): 467-473.
34. Gyongyosi, Laszlo. Linear optical quantum computing with photonic qubits. *Rev Mod Phys* 79(2007): 135-174.
35. Gisin, Nicolas, and Rob Thew. Quantum Communication. *Nature Photon* 1(2007): 165-171.
36. Van Enk. Photonic channels for quantum communication. *Science* 279(1998): 205-208.
37. Briegel, HJ, Wolfgang Dür, Juan I Cirac, and Peter Zoller. Quantum repeaters: the role of imperfect local operations in quantum communication. *Phys Rev Lett* 81(1998): 5932-5935.
38. Dür, W, HJ Briegel, J Ignacio Cirac, and P Zoller. Quantum repeaters based on entanglement purification. *Phys Rev A* 59(1999): 169-181.
39. Duan, LM, Mikhail D Lukin, J Ignacio Cirac, and Peter Zoller. Long-distance quantum communication with atomic ensembles and linear optics. *Nature* 414(2001): 413-418.
40. Van Loock, P, TD Ladd, Kaoru Sanaka, and F Yamaguchi, et al. Hybrid quantum repeater using bright coherent light. *Phys Rev Lett* 96(2006): 240501.
41. Zhao, Bo, Zeng-Bing Chen, Yu-Ao Chen, and Jörg Schmiedmayer, et al. Robust creation of entanglement between remote memory qubits. *Phys Rev Lett* 98(2007): 240502.
42. Müller, Simon. Flexible heuristic algorithm for automatic molecule fragmentation: application to the UNIFAC group contribution model. *J Cheminform* 11(2019): 57.

How to cite this article: Grigoriadis, Ioannis. "Topology Geometrics for the Generation of the Roccustyrnatm Molecule, A Ligand Targeted Covid-19-D614g Sites.1." *Clin Schizophr Relat Psychoses* Spl 1(2020)